이학박사학위논문

The Physics of a Ring Polymeric Melt: from Structure to Dynamics

원형 고분자 용융의 구조 및 동역학 연구

2015 년 8 월

서울대학교 대학원
화학부
이 은 상

The Physics of a Ring Polymeric Melt: from Structure to Dynamics

Eunsang Lee

Supervised by
Professor **YounJoon Jung**

A Dissertation
Submitted to the Faculty of
Seoul National University
in Partial Fulfillment of
the Requirements for the Degree of
Doctor of Philosophy
July 2015

Department of Chemistry
Graduate School
Seoul National University

Abstract

A ring polymer is one of the novel topological classes in polymer physics. Unlike linear and branched polymers, its two ends are connected to each other, thus two intrinsic constraints, non-knotting and non-concatenation inhere in the ring polymer. Due to these constraints, a ring in a melt phase adopts a compact globular structure with high fractal dimension. Interestingly, the structure of a ring in a melt resembles chromosomes in eukaryotic nuclei during the interphase. Although a chromatin fiber is a polymer with open ends, its structure in a nucleus seems not tangled to each other. Therefore, to understand the nature of the chromosome packing, it is instructive to study the physics of a ring in a melt from the polymer physics point of view.

In this thesis, we first present a theory and molecular dynamics simulation results for the ring polymer melt structure in a bulk phase. Unlike a linear polymer, it is found that the Flory exponent of a ring varies from 1/2 to 1/3 as degree of polymerization increases. Especially for longer rings, it turns out that compact and segregated structures are favored due to the topological constraints. A theoretical study of Flory-type free energy minimization by considering the topological constraints as an effective excluded volume supports the numerical results.

We also study structural properties of a ring polymeric melt confined in a film in comparison to a linear counterpart using molecular dynamics simula-

tions. Local structure orderings of ring and linear polymers in the vicinity of the surface are similar to each other because the length scale of surface-monomer excluded volume interaction is smaller than the size of an ideal blob of the ring. In a long length scale, while the Silberberg hypothesis can be used to provide a physical origin of confined linear polymer results, it no longer holds for a ring polymer case. We also present different structural properties of ring and linear polymers in a melt, including the size of polymers, an adsorbed amount, and the coordination number of a polymer. Our observation reveals that a confined ring in a melt adopts highly segregated conformation due to a topological excluded volume repulsion.

In addition to the structural studies, we investigate the origin of the slow dynamics of ring polymer melts. Diffusion of long ring polymers in a melt is shown to be much slower than the reorganization of their internal structures. While a direct evidence for entanglements has not been observed in the log ring polymers unlike linear polymer melts, threading between the rings is suspected to be the main reason for slowing down of ring polymer diffusion. It is, however, difficult to define the threading configuration between two rings because the rings have no chain end. In this thesis, an evidence for threading dynamics of ring polymers is presented by using molecular dynamics simulation and applying a novel analysis method. The simulation results are analyzed in terms of the statistics of persistence and exchange times that have been proved useful in studying heterogeneous dynamics of glassy systems. It is found that the threading time of ring polymer melts increases more rapidly with the degree of polymerization than that of linear polymer melts. This indicates that threaded

ring polymers cannot diffuse until an unthreading event occurs, which results in the slowing down of ring polymer diffusion.

These studies for structures and dynamics of the ring polymer melts provide not only a new perspective to understand an unsolved problem in biological system, but a possibility to utilize new materials with novel viscoelastic properties.

Keywords: ring polymer, correlation hole, topological constraints, segregation, fractal globule, Silberberg hypothesis, threading dynamics, entanglement effect, non-knotting, non-concatenation, chromosome packing, persistence/exchange time

Student Number: 2008-22732

Contents

List of Figures

List of Tables

Chapter 1

Overview

A polymer is a macromolecule consisting of repeated subunits, called monomers. Due to wide applications of polymers in the fields of industry, engineering, medical science, and *etc.*,[1–3] understanding polymer properties has emerged as a big challenge to many scientists for over a decade. Especially, theoretical backgrounds for the polymer physics have served great intuitions for designing polymers with desired structural, mechanical and dynamical properties.[4–6]

In polymer physics, polymers are usually classified by topology *i.e.*, overall connectivity. Polymers belonging to each topological class show universal properties regardless of the chemical details in given conditions such as temperature, density, and solvent quality. Linear, branched, and ring polymers are examples of the topological classes in polymer physics. It is shown that in a given environment, the sizes of polymers R, *e.g.*, radius of gyration, follow a

power law with respect to degree of polymerization N (the number of monomers in a molecule), $R \sim N^{\nu}$. Such a structure showing the power law between the mass and the size in nature is usually called a fractal, and a fractal dimension is defined by the exponent in the power law (in polymers, fractal dimension is $1/\nu$). Therefore, one of the most fundamental questions in polymer physics is to obtain the fractal dimension for each topological polymer class in a given environment. For example, an ideal linear chain whose monomers are assumed not to interact with each other can be represented by a random walk, which is characterized by $R \sim N^{1/2}$.[6] It is also well known that solvent quality affects the fractal dimension of a linear polymer solution, which varies from $\nu \approx 3/5$ for a good solvent to for $\nu = 1/3$ a poor solvent.

Recently, physicists and biologists have taken an interest in a novel interesting topological polymer class-a ring. Its both ends are connected to each other, *i.e.* it has no chain end. One can easily find the macromolecules with circular morphologies in biological systems, such as circular DNAs found in bacteria, viruses as well as in eukaryotic cells.[7] It is also fascinating that an image of chromosomal territories in a nucleus resembles a snapshot of molecular dynamics computer simulations for ring polymer melts.[8] Despite their importance in biological systems as well as industries, ring polymers have been investigated mainly by means of theories and computer simulations, since it is not easy to synthesize monodisperse ring polymers in laboratories.[9]

In this thesis, therefore, we study structural and dynamical properties of ring polymers in a melt phase via molecular dynamics (MD) simulations and theories. The polymer melt is a neat polymeric liquid without any solvent

molecule. It has viscoelastic properties, which means that it behaves like an elastic material in short time scale but shows a viscous diffusion in long time scale. Compared to the linear polymer melts whose behavior is well understood by a huge number of experiments, simulations and theories, only a few number of articles have been published to elucidate the structures and dynamics of ring polymer melts. Therefore, we study the structures and dynamics of ring polymer melts not only to understand the physics of ring polymer melts but to provide an intuition for biological phenomena including chromosomal territories in an interphase nucleus.

This thesis is organized as follows. In Chap. 2, we briefly review theories for linear polymer melts. Recalling the physics of linear polymer melts, such as ideal chain statistics, Rouse model, and reptation model, is essential to understand ring polymer physics. In Chap. 3, a theory and the simulation results for the ring polymer melt in a bulk phase are provided. Next, we present structures of ring polymer melts in a confined geometry compared to its linear counterpart in Chap. 4. Interesting relations between scaling exponents are shown by simulations and theories. In Chap. 5, we study dynamics of ring polymers in a melt, which is known to show an uncoupled diffusion-reorganization behavior. We prove that this abnormal behavior is caused by an inter-ring threading in terms of exchange and persistence time distributions in MD simulations. Conclusion remark follows in the final chapter.

Chapter 2

Review on Polymer Physics

In this chapter, we provide a brief review on polymer physics especially focusing on the linear polymers. While a number of textbooks have dealt with this subject,[4–6] recalling the theories for the linear polymers would be useful to understand the physics of ring polymers in following chapters. Here, we first show the static properties of linear polymers as the monomer excluded volume interaction changes. Rouse and reptation models follow to explain the dynamics of linear polymers in a melt.

2.1 Structures of Linear Polymers

2.1.1 Ideal Chain

Let us start with a very simple model, freely jointed chain (FJC) model, which consists of massless points connected by bonds with a constant length, l. The

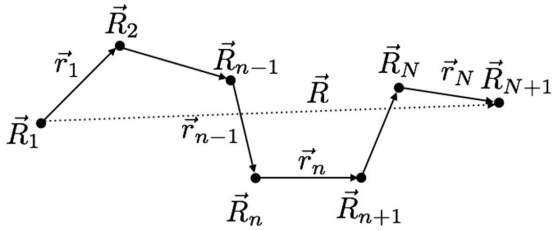

Figure 2.1 Schematic description of a freely jointed chain model. $\vec{R}_n$ is the position vector of an n-th monomer and $\vec{r}_n$ is the n-th bond vector. $\vec{R}$ represents the size of the chain.

bonds are free to rotate. This model is analogous to the random walk in three dimension in which the length of a step is l. Figure 2.1 shows schematic description of the FJC. Here, the bond vector is represented by: $\vec{r}_n = \vec{R}_{n+1} - \vec{R}_n$, where $\vec{R}_n$ is the position vector of an n-th monomer, and $|\vec{r}_n| = l$ for all n. In this model, the ensemble average of end-to-end distances $\langle \vec{R} \rangle$ can be written as

$$< \vec{R} >= \sum_{i=1}^{N} \vec{r}_i = 0, \tag{2.1}$$

and and ensemble average of squared end-to-end distances is:

$$\begin{aligned} \langle R^2 \rangle = \langle \vec{R}^2 \rangle &= \left\langle \left(\sum_{i=1}^{N} \vec{r}_i \right) \left(\sum_{j=1}^{N} \vec{r}_j \right) \right\rangle \\ &= \sum_{i}^{N} \sum_{j}^{N} \langle \vec{r}_i \cdot \vec{r}_j \rangle \\ &= \sum_{i}^{N} \sum_{j}^{N} l^2 \cos\theta_{ij} \\ &= Nl^2 + 2l^2 \sum_{i}^{N} \sum_{j>i}^{N} \cos\theta_{ij}, \end{aligned} \tag{2.2}$$

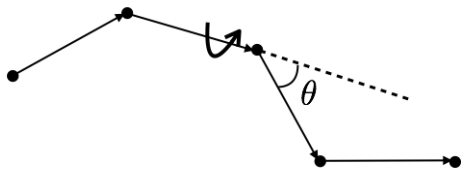

Figure 2.2 Schematic description of a freely rotating chain model. θ is the bond angle between two adjacent bond vectors.

where θ_{ij} is an angle between two bond vectors, $\vec{r}_i$ and $\vec{r}_j$. For FJC model, $\cos\theta_{ij} = 1$ for $i = j$ and 0 for $i \neq j$, thus Eqn. 2.2 arrives at $\langle \vec{R}^2 \rangle = Nl^2$. It is instructive to keep in mind that an average of squared end-to-end distance is proportional to N^1.

As mentioned above, the FJC model can be considered as the random walk in three dimension, in which $\vec{R}$ is the position after N random steps. Therefore, a probability distribution for the end-to-end vector $\vec{R}$ of FJC model with N monomers follows a normal distribution in analogy to the random walk:

$$P(N, \vec{R}) = \left(\frac{3}{2\pi N b^2} \right)^{3/2} \exp\left(- \frac{3\vec{R}^2}{2Nb^2} \right). \tag{2.3}$$

Using this equation, we can reproduce $\langle R^2 \rangle = \int \vec{R}^2 P(N, \vec{R}) \mathrm{d}^3\vec{R} = Nb^2$.

For real polymers, however, there is normally a correlation between two bond vectors, in other words, $\cos\theta_{ij} \neq 0$ for $i \neq j$. One of the simplest models to mimic the correlation between bond vectors is the freely rotating chain (FRC) model. In this model, the bond length is constant as well as in the FJC and the bonds are free to rotate with fixed angle, θ, between two adjacent bond vectors (Fig. 2.2). An ensemble average of squared end-to-end distances for this model

is calculated as:

$$\begin{aligned}
\langle R^2 \rangle &= Nl^2 + 2l^2 \sum_i^N \sum_{j>i}^N \cos\theta_{ij} \\
&= Nl^2 + 2l^2 \sum_i^N \sum_{j>i}^N \cos^{|j-i|}\theta \\
&= Nl^2 + 2l^2 \sum_i^N \sum_k^{N-i} \cos^k\theta \\
&\approx Nl^2 + 2l^2 \sum_i^N \sum_k^{\infty} \cos^k\theta \\
&= Nl^2 + 2Nl^2 \frac{\cos\theta}{1-\cos\theta} \\
&= Nl^2 \frac{1+\cos\theta}{1-\cos\theta}.
\end{aligned} \tag{2.4}$$

In this equation, we use an approximate relation, $\sum_k^{N-i} \cos^k\theta \approx \sum_k^{\infty} \cos^k\theta$, since $\cos^k\theta$ rapidly converges to zero. The stiffness of chains is characterized by the persistence length, l_p. For the FRC model, $\langle \vec{r}_i \cdot \vec{r}_j \rangle = l^2 \cos\theta_{ij} = l^2 \cos^{|j-i|}\theta$ decays to zero as a contour length, $l|j-i|$, increases (Fig. 2.3). If we set the persistence length to $l_\mathrm{p}/l = -1/\ln(\cos\theta)$, then we obtain exponential decay of $\langle \vec{r}_i \cdot \vec{r}_j \rangle$, such that: $\langle \vec{r}_i \cdot \vec{r}_j \rangle / l^2 = \exp(-l|j-i|/l_\mathrm{p})$.

It is very important to note that since the FRC model also gives the squared end-to-end distance proportional to N^1 as well as the FJC model, we can consider FRC as FJC, using the equation:

$$\langle R^2 \rangle = Nl^2 \frac{1+\cos\theta}{1-\cos\theta} = N'b^2. \tag{2.5}$$

The segment of FJC in the FRC model is usually called Kuhn monomer, and the size of the Kuhn monomer is Kuhn length. In Eqn.2.5, N' is the number of Kuhn segments in a polymer. Using the relation of the maximum extension

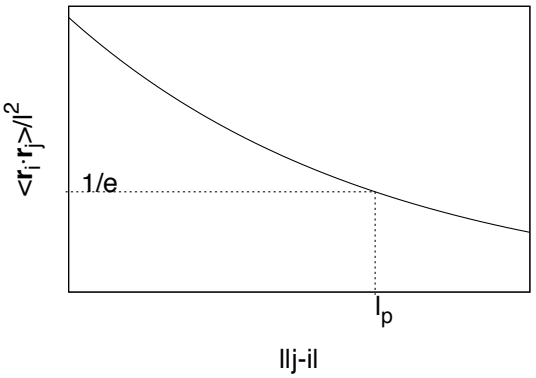

Figure 2.3 Inner product of two bond vectors $\vec{r}_i \cdot \vec{r}_j$ divided by l^2 as a function of a contour length, $l|j-i|$. Dashed lines represent $1/e$ and a persistent length $l_{\rm p}$.

of the chain, $R_{\max} = Nl = N'b$, the Kuhn length, b, and the number of Kuhn segments, N' are obtained by:

$$b = l\frac{1+\cos\theta}{1-\cos\theta}, \tag{2.6}$$

$$N' = N\frac{1-\cos\theta}{1+\cos\theta}. \tag{2.7}$$

For chains with a small bond angle, usually called worm-like chain model, the persistence length and the Kuhn length can be obtained using Taylor expansion. If one ignores the second and higher order terms, one can obtain $b = 4l/\theta^2 = 2l_{\rm p}$. A double-helical DNA is properly modeled by the worm-like chain model, and it is well known to have $l_{\rm p} \approx 50$nm and $b \approx 100$nm. From now on, we only discuss the polymers composed of N Kuhn segments with size b. One should keep in mind that any homopolymer can be considered to such a freely jointed polymer model.

The end-to-end distance is a well-defined observable for a linear polymer as mentioned above, but it cannot characterize the size of branched and ring polymers. Instead, radius of gyration, $R_{\rm g}$ is widely used to study the static properties of polymers as well as the end-to-end distance. The squared radius of gyration is defined by

$$R_{\rm g}^2 = \frac{1}{N}\sum_{i=1}^{N}(\vec{R}_i - \vec{R}_{\rm CM})^2 = \frac{1}{N}\sum_{i=1}^{N}\sum_{j=i}^{N}(\vec{R}_i - \vec{R}_j)^2, \tag{2.8}$$

where i is the monomer index and N is the number of Kuhn monomers. The last equality in Eqn. 2.8 uses the definition of the center of mass position vector, $\vec{R}_{\rm CM} = (1/N)\sum_{i=1}^{N}\vec{R}_i$. For the ideal chain, an ensemble average of squared gyration radii is calculated by,

$$\begin{aligned}
\langle R_{\rm g}^2\rangle &= \frac{1}{N}\sum_{i=1}^{N}\sum_{j=i}^{N}\langle(\vec{R}_i - \vec{R}_j)^2\rangle \\
&= \frac{1}{N}\sum_{i=1}^{N}\sum_{j=i}^{N}(j-i)b^2 \\
&\approx \frac{b^2}{N^2}\int_0^N {\rm d}x\int_x^N {\rm d}y(y-x) \\
&= \frac{N}{6}b^2.
\end{aligned} \tag{2.9}$$

We also obtain a relation between the mean-squared radius of gyration and the mean-squared end-to-end distance, $\langle R_{\rm g}^2\rangle = \langle R^2\rangle/6$.

2.1.2 Excluded Volume and Real Chains

Up to now, we have discussed the ideal chain model, in which the interaction between points (monomers) in a chain is ignored. However, for real polymers, the monomer-monomer interaction perturbs the chain structure from the ideal

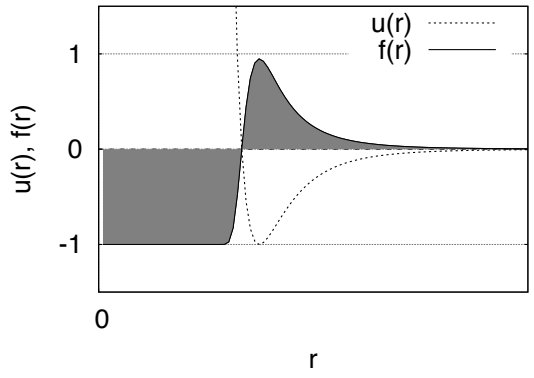

Figure 2.4 Graphical illustrations for a pairwise monomer-monomer interaction (dotted line, $u(r)$), Mayer f-function (solid line, $f(r)$), and the monomer-monomer excluded volume (shaded area, $v_{\rm ex}$).

one. The most useful parameter to characterize this interaction strength is a monomer excluded volume, $v_{\rm ex}$. Let us consider an effective pairwise interaction between two monomers, $u(r)$. Mayer f-function widely used in statistical mechanics of liquids is defined by $f(r) = \exp[-u(r)/k_{\rm B}T] - 1$. The monomer-monomer excluded volume can then be defined by:

$$v_{\rm ex} = -\int_0^\infty f(r)\mathrm{d}^3r = \int_0^\infty \big(1 - \exp[-u(r)/k_{\rm B}T]\big)\mathrm{d}^3r \cong v_{\rm ex}^0\left(1 - \frac{\theta}{T}\right). \quad (2.10)$$

The last equality in this equation is useful in experiments to characterize the solvent quality or the temperature which affect the polymer statistics. θ is a temperature at which the excluded volume equals zero. $v_{\rm ex}^0$ is the excluded volume at the infinite temperature (athermal condition). Figure 2.4 shows the graphical representation of a pairwise monomer-monomer interaction, Mayer f-function, and the monomer-monomer excluded volume.

Let us consider a polymer solution. If monomers are likely to be in contact to each other, the effective monomer-monomer interaction is attractive. In this case, the interaction potential has a deep attractive well which results in the negative excluded volume. A solvent satisfying this condition is called a poor solvent. In contrast, if the effective interaction is repulsive, the excluded volume is positive. A solvent in this condition is called a good solvent. If the solvent quality is in between the good and poor solvents, the excluded volume is exactly zero due to cancellation between the repulsive and attractive potentials. The solvent satisfying this condition is called a θ-solvent. A polymer in the θ-solvent or at the θ-temperature follows, of course, an ideal chain statistics.

The size of a polymer in a good solvent can be calculated by mean-field approach usually called Flory theory. The free energy for a polymer of degree of polymerization N having the size R is contributed by two terms. The first one is the energetic cost, $F_{\mathrm{eng}}(N, R)$, which is the free energy penalty that the monomer of the excluded volume v_{ex} is located in the volume of the polymer R^3. Since there are N monomers in the volume R^3, the energy cost per a monomer is $k_{\mathrm{B}}Tv_{\mathrm{ex}}N/R^3$ and finally,

$$F_{\mathrm{eng}}(N) = k_{\mathrm{B}}Tv_{\mathrm{ex}}N^2/R^3. \tag{2.11}$$

The second contribution to the free energy is an entropic cost, $F_{\mathrm{ent}}(N, R)$. The entropy loss due to the chain extension is proportional to the number of microstate of a polymer, which is determined by the probability distribution of the chain size, $P(N, \vec{R})$ (Eqn. 2.3). If the chain size is slightly perturbed from

the ideal one, we obtain an entropy upon stretching of the chain to the size R:

$$F_{\mathrm{ent}}(N,R) = -TS(N,R) \approx -k_{\mathrm{B}}T \ln P(N,\vec{R}) = \frac{3k_{\mathrm{B}}T}{2b^2}\frac{\vec{R}^2}{N}. \tag{2.12}$$

Therefore, the total free energy of a polymer in a good solvent is the sum of two contributions:

$$F(N,R) = F_{\mathrm{eng}}(N,R) + F_{\mathrm{ent}}(N,R) \approx k_{\mathrm{B}}T\left(v_{\mathrm{ex}}\frac{N^2}{R^3} + \frac{3R^2}{2Nb^2}\right). \tag{2.13}$$

By minimizing the free energy with respect to R, we obtain the size:

$$R \approx v_{\mathrm{ex}}^{1/5} b^{2/5} N^{3/5} \sim N^{3/5}. \tag{2.14}$$

As well as the ideal chain, the size of polymers in a good solvent follows a power law with respect to the degree of polymerization, N, such that $R \sim N^{\nu}$, in which ν is called Flory exponent. A chain in a good solvent swells with $\nu = 3/5$ and its size is larger than the ideal counterpart. The swelling ratio to the ideal chain size is:

$$\frac{v_{\mathrm{ex}}^{1/5} b^{2/5} N^{3/5}}{bN^{1/2}} = \left(\frac{v_{\mathrm{ex}}N^{1/2}}{b^3}\right)^{1/5} = z^{1/5}, \tag{2.15}$$

where the chain interaction parameter is defined by $z \equiv v_{\mathrm{ex}}N^{1/2}/b^3$. Compared to the random walk statistics of the ideal chain, a polymer in a good solvent can be represented by the self-avoiding walk (SAW) in which monomers repel each other due to the monomer excluded volume. Flory-type free energy minimization procedure has been widely applied to various polymer types, although the above calculation gives a good agreement with experiments due to the fortunate cancellation between overestimated energy and entropic terms. More sophisticated renormalization calculation states that $\nu = 0.588$.

Flory-type free energy minimization can predict statistics of a polymer in a poor solvent as well. We first get a virial expansion of the energetic contribution of the free energy density in terms of the monomer density, N/R^3:

$$\frac{F_{\text{eng}}}{R^3} = k_{\text{B}}T\left[B_2\left(\frac{N}{R^3}\right)^2 + B_3\left(\frac{N}{R^3}\right)^3 + \cdots\right], \tag{2.16}$$

where B_i is an i-th virial coefficient. The ideal term is ignored since we only consider relative free energy change from the ideal state. Note that if we let $B_2 = v_{\text{ex}}$, the first term arrives at exactly the energetic cost of the free energy of a polymer in the good solvent in Eqn. 2.11. In a good solvent condition, the monomer density is small enough to ignore the third virial term representing the three-body interaction. However, a polymer in the poor solvent has a high monomer density since $R < bN^{1/2}$, therefore the three-body interaction term should be considered when calculating F_{eng}. Combining the entropic contribution in Eqn. 2.12 with Eqn. 2.16, we can obtain the free energy:

$$\begin{aligned} F(N,R) &= F_{\text{eng}}(N,R) + F_{\text{ent}}(N,R) \\ &\approx k_{\text{B}}T\left[v_{\text{ex}}\frac{N^2}{R^3} + w\frac{N^3}{R^6} + \frac{3R^2}{2Nb^2}\right] \\ &\approx k_{\text{B}}T\left[v_{\text{ex}}\frac{N^2}{R^3} + w\frac{N^3}{R^6}\right], \end{aligned} \tag{2.17}$$

where $w = B_3$ is the three-body interaction coefficient. The last equality uses the approximation of $R < bN^{1/2}$. Minimization of Eqn. 2.17 with respect to R gives the size of polymers in a poor solvent:

$$R \approx \left(\frac{w}{|v_{\text{ex}}|}\right)^{1/3} N^{1/3}. \tag{2.18}$$

In this equation, $v_{\text{ex}} < 0$ because of the poor solvent condition. The typical value of three-body interaction coefficient is $w = b^6$, thus Eqn. 2.18 reduces to

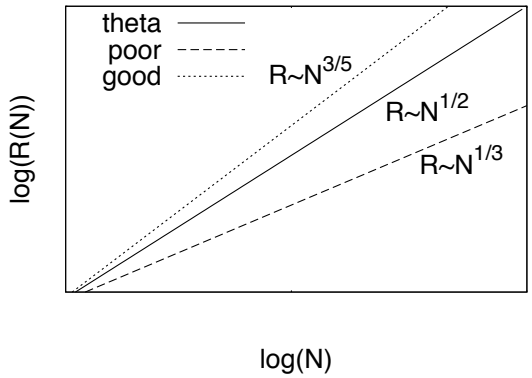

Figure 2.5 Power law behaviors of polymer size in theta(solid line), good(dotted line), and poor solvents(dashed line). Flory exponents in each condition is represented in the figure.

$R \approx |v_{\mathrm{ex}}|^{-1/3} b^2 N^{1/3}$. A polymer in the poor solvent has a smaller size and a more compact structure than the ideal chain, which is characterized by small Flory exponent, 1/3. Such a structure is usually called a globule. Figure 2.5 shows log-log plots of polymer sizes as a function of degree of polymerization in various solvent conditions.

2.1.3 Flory-Huggins Theory

In this section, we derive a free energy change when the two polymers are mixed, which is called Flory-Huggins equation. Let us consider a two-dimensional square lattice system containing polymers A and B which follow a self-avoiding walk. Each lattice site mimics a monomer and all lattice sites are occupied by monomers. The polymer A consists of N_{A} monomers, and the polymer B consists of N_{B} monomers. The numbers of A and B polymers are n_{A} and n_{B},

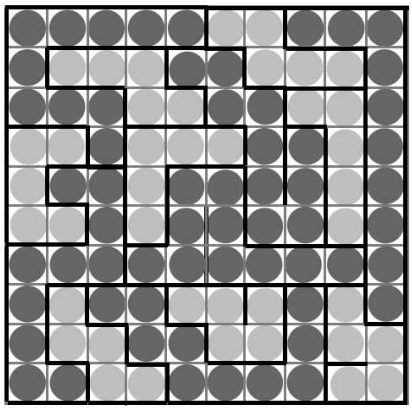

Figure 2.6 A lattice model for a polymer blend. In this figure, the polymer A consists of $N_A = 10$ monomers and the polymer B consists of $N_B = 5$ monomers. The number of A and B polymers are $n_A = 6$, and $n_B = 8$, respectively.

respectively. The volume fractions of polymer A and B are:

$$\phi_{\rm A} = \frac{n_{\rm A} N_{\rm A}}{n_{\rm A} N_{\rm A} + n_{\rm B} N_{\rm B}}, \qquad \phi_{\rm B} = 1 - \phi_{\rm A} = \frac{n_{\rm B} N_{\rm B}}{n_{\rm A} N_{\rm A} + n_{\rm B} N_{\rm B}}. \tag{2.19}$$

The total number of lattice sites is $N_{\rm tot} = n_{\rm A} N_{\rm A} + n_{\rm B} N_{\rm B}$.

The entropy of mixing can be calculated as follows. The entropy is proportional to logarithm of the number of possible microstates Ω, and Ω of each species is proportional to the number of lattice sites. Therefore, the entropy change of A polymers upon mixing is:

$$\begin{aligned} \Delta S_{\rm A} &= n_{\rm A}(S_{\rm A,mixed} - S_{\rm A,unmixed}) \\ &= n_{\rm A} k_{\rm B} \ln \frac{\Omega_{\rm A,mixed}}{\Omega_{\rm A,unmixed}} \\ &= n_{\rm A} k_{\rm B} \ln \frac{N_{\rm tot}}{n_{\rm A} N_{\rm A}} \\ &= -n_{\rm A} k_{\rm B} \ln \phi_{\rm A}. \end{aligned} \tag{2.20}$$

Obviously, the entropy change of B polymers upon mixing is $\Delta S_{\rm B} = -n_{\rm B}k_{\rm B}\ln\phi_B = -(1-n_{\rm A})k_{\rm B}\ln(1-\phi_{\rm A})$. Therefore, the total entropy change upon mixing is $\Delta S = -k_{\rm B}(n_{\rm A}\ln\phi_{\rm A} + n_{\rm B}\ln\phi_{\rm B})$ and the entropy of mixing is:

$$\Delta S = -N_{\rm tot}k_{\rm B}\left[\frac{\phi_{\rm A}}{N_{\rm A}}\ln\phi_{\rm A} + \frac{\phi_{\rm B}}{N_{\rm B}}\ln\phi_{\rm B}\right]. \tag{2.21}$$

Here, we use a relation $n_{\rm A} = N_{\rm tot}\phi_{\rm A}/N_{\rm A}$ and $n_{\rm B} = N_{\rm tot}\phi_{\rm B}/N_{\rm B}$. The volume fractions of two species are smaller than unity. Therefore, the entropy change is always positive which promotes mixing.

Next, we derive the energy of mixing. In the unmixed state, if the interaction energy between two monomers of the polymer A is $u_{\rm A}{}_A$ then the average energy of the unmixed polymer A is $U_{\rm A,unmixed} = zN_{\rm tot}\phi_{\rm A}u_{\rm AA}/2$, where z is the coordination number, $z = 4$ for the square lattice in this theory. Factor 2 in denominator accounts for the double counting. Similarly, $U_{\rm B,unmixed} = zN_{\rm tot}\phi_{\rm B}u_{\rm BB}/2$. Therefore, the energy before mixing is:

$$U_{\rm unmixed} = U_{\rm A,unmixed} + U_{\rm B,unmixed} = \frac{zN_{\rm tot}}{2}(u_{\rm AA}\phi_{\rm A} + u_{\rm BB}\phi_{\rm B}) \tag{2.22}$$

In the mixed state, the probabilities of a monomer of a polymer A being in a contact with other monomers of the polymer A and B are $\phi_{\rm A}$ and $\phi_{\rm B}$, respectively. Thus, the average energy of the mixed polymer A is $U_{\rm A,mixed} = zN_{\rm tot}\phi_{\rm A}(u_{\rm AA}\phi_{\rm A} + u_{\rm AB}\phi_{\rm B})/2$, where $u_{\rm AB}$ is the interaction energy of A and B monomers. $U_{\rm B,mixed} = zN_{\rm tot}\phi_{\rm A}(u_{\rm AA}\phi_{\rm A} + u_{\rm AB}\phi_{\rm B})/2$, so the total energy in the mixed state is:

$$\begin{aligned} U_{\rm mixed} &= U_{\rm A,mixed} + U_{\rm B,mixed} \\ &= \frac{zN_{\rm tot}}{2}(u_{\rm AA}\phi_{\rm A}^2 + 2u_{\rm AB}\phi_{\rm A}\phi_{\rm B} + u_{\rm B}{}_B\phi_{\rm B}^2). \end{aligned} \tag{2.23}$$

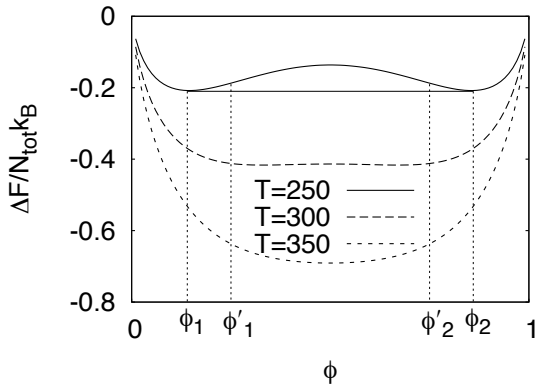

Figure 2.7 A free energy of mixing for a polymer blend with $N_{\rm A} = N_{\rm B} = 100$ and $\chi = 5/T$.

Therefore, the energy of mixing is:

$$\begin{aligned} \Delta U &= U_{\rm mixed} - U_{\rm unmixed} \\ &= \frac{zN_{\rm tot}}{2}\phi_{\rm A}\phi_{\rm B}(2u_{\rm AB} - u_{\rm AA} - u_{\rm BB}) \\ &= k_{\rm B}T\chi\phi_{\rm A}\phi_{\rm B}. \end{aligned} \tag{2.24}$$

Here, we define a Flory-Huggins parameter, χ, by:

$$\chi \equiv \frac{z}{2k_{\rm B}T}(2u_{AB} - u_{\rm AA} - u_{\rm BB}). \tag{2.25}$$

If the polymer A and polymer B like each other more than themselves, $2u_{\rm AB} < u_{\rm AA} + u_{\rm BB}$ which results in negative χ, and a single phase is favored. In contrast, if $\chi > 0$, two polymers do not tend to intermixed and the phase separation occurs.

Finally, we can obtain the free energy change upon mixing two polymers:

$$\Delta F = \Delta U - T\Delta S = N_{\rm tot}k_{\rm B}T\left[\frac{\phi_{\rm A}}{N_{\rm A}}\ln\phi_{\rm A} + \frac{\phi_{\rm B}}{N_{\rm B}}\ln\phi_{\rm B} + \chi\phi_{\rm A}\phi_{\rm B}\right], \tag{2.26}$$

which is called the Flory-Huggins equation. If we let $N_{\mathrm{A}} = N$ and $N_{\mathrm{B}} = 1$, Eqn. 2.26 arrives at the equation describing the free energy of mixing for a polymer solution. Figure 2.1.3 shows the free energy of mixing of two polymers with $N_{\mathrm{A}} = N_{\mathrm{B}} = 100$ and $\chi = 5/T$. At $T = 300\mathrm{K}$, a homogeneous phase are stable with the composition of $\phi_{\mathrm{A}} = \phi_{\mathrm{B}} = 0.5$. As the temperature is lowered, unstable region where the second derivative of ΔF is positive starts to appear. At $T = 200\mathrm{K}$, there are two compositions at which $\partial^2 \Delta F/\partial \phi_{\mathrm{A}}^2|_{\phi_{\mathrm{A}}=\phi_1'} = \partial^2 \Delta F/\partial \phi_{\mathrm{A}}^2|_{\phi_{\mathrm{A}}=\phi_2'} = 0$. In between these two compositions, homogeneous phase is unstable and coexistence of two phases of $\phi_{\mathrm{A}} = \phi_1$ and $\phi_{\mathrm{A}} = \phi_2$ is observed. Here, ϕ_1 and ϕ_2 are obtained by a the common tangent line.

2.1.4 Linear Polymer Melts

From now on, we discuss linear polymers in a melt phase. The melt phase means a very condensed liquid phase of polymers without any solvent molecule. In order to calculate the excluded volume of the linear polymer in a melt, let us consider a polymer melt as a polymer blend composed of one "distinguishable" polymer molecule (A) and other polymers of the same species (B). For this case, because the volume fraction of A is very small compared to that of B ($\phi_{\mathrm{A}} << 1$), Eqn. 2.26 can be written as:

$$\Delta F \approx N_{\mathrm{tot}} k_{\mathrm{B}} T \left[\frac{\phi_{\mathrm{A}}}{N_{\mathrm{A}}} \ln \phi_{\mathrm{A}} + \phi_{\mathrm{A}} \left(\chi - \frac{1}{N_{\mathrm{B}}} \right) + \frac{\phi_{\mathrm{A}}^2}{2} \left(\frac{1}{N_{\mathrm{B}}} - 2\chi \right) + \cdots \right]. \quad (2.27)$$

By comparing this with Eqn. 2.16, the second virial coefficient which is considered as the excluded volume is the coefficient in front of the second order term with respect to ϕ_{A} in Eqn. 2.27. Therefore, we approximately obtain the

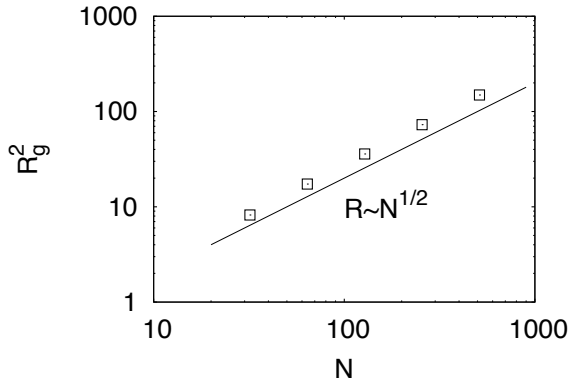

Figure 2.8 Radius of gyration as a function of degree of polymerization obtained by simulations of a bead-spring model. Thin line represents the scaling of $R_{\rm g} \sim N^{1/2}$.

excluded volume of the linear polymer melt, such that:

$$v_{\rm ex} \approx \left(\frac{1}{N_{\rm B}} - 2\chi\right) b^3 \tag{2.28}$$

This equation can be exactly obtained by an osmotic pressure which is calculated by differentiating the free energy of mixing with respect to a volume of the system[6] (not shown here).

Interestingly, χ for this system is zero because two species, A and B, are identical, thus $v_{\rm ex} \approx b^3/N_{\rm B}$. Usually, $N_{\rm B} >> b^3$ which leads to $v_{\rm ex} \approx 0$. This means that interaction between monomers in a reference polymer (A) is screened out by other monomers belonging to penetrating polymers (B) inside the pervaded volume of the reference polymer. As a result, linear polymers in the melt phase behave like an ideal chain. Figure 2.1.4 shows the radius of gyration as a function of degree of polymerization, which is obtained by molecular dynamics simula-

tions of a bead-spring model. This figure clearly shows that the size of a polymer is proportional to $N^{1/2}$ as well as in Eqn. 2.9. Simulation details and other interesting characteristics of linear polymer melts will be discussed in remained parts of the thesis.

2.2 Dynamics of Linear Polymers

One more interesting feature of linear polymers in a melt is their dynamic behavior. In order to understand the dynamics of linear polymer melts, we first briefly explain the dynamics of a small colloidal particle in a liquid, which diffuses through the liquid due to the thermal fluctuation. For such a random walk in three dimension, it is well known that a squared particle displacement is proportional to diffusion coefficient D, and a time t, such that:

$$\langle \big(\vec{r}(t) - \vec{r}(0)\big)^2 \rangle = 6Dt. \tag{2.29}$$

The particle following such a simple diffusive motion is usually called a Brownian particle. Moreover, the diffusion coefficient is related as Einstein relation:

$$D = \frac{k_{\mathrm{B}}T}{\zeta}, \tag{2.30}$$

where ζ is friction coefficient which relating the force acting on the particle to the particle velocity. Another useful relation is Stokes relation:

$$\zeta = 6\pi\eta R, \tag{2.31}$$

where η is a viscosity of the solvent and R is a hydrodynamic radius of the solvent. By combining these two equations, we obtained Stokes-Einstein relation:

$$D = \frac{k_{\mathrm{B}}T}{6\pi\eta R}. \tag{2.32}$$

Table 2.1 Summary of dynamic properties of Rouse and Reptation models.

Properties	Notation	Rouse	Reptation
Self-diffusion coefficient	D	$\sim N^{-1}$	$\sim N^{-2}$
Longest relaxation time	τ	$\sim N^{2}$	$\sim N^{3}$
Stress relaxation modulus	$G(t)$	$\sim t^{-1/2}$	Plateau modulus
Viscosity	η	$\sim N^{1}$	$\sim N^{2}$

Following the relation, we can obtain the characteristic time scale of diffusion τ, which is the time required for the Brownian particle move a distance of order of its own size R:

$$\tau \approx \frac{R^2}{D} \approx \frac{R^2 \zeta}{k_{\mathrm{B}} T}. \tag{2.33}$$

Here, the time scale for diffusive motion is proportional to the friction coefficient.

2.2.1 Rouse Model

Dynamics of linear polymers is modeled by N beads connected by massless, frictionless springs. Such a model is usually called the Rouse model. In this model, each bead has a friction ζ, and the friction of a polymer is expressed by the sum of frictions of whole beads, $N\zeta$. As a result, the diffusion coefficient of a polymer is obtained by the Einstein relation:

$$D \approx \frac{k_{\mathrm{B}} T}{N \zeta}. \tag{2.34}$$

The time scale required for the linear polymer in a melt to move a distance of an order of its size is:

$$\tau \approx \frac{R^2}{D} \approx \frac{N\zeta R^2}{k_{\mathrm{B}}T} \approx \frac{\zeta b^2 N^2}{k_{\mathrm{B}}T}, \tag{2.35}$$

which is called the Rouse time. Above equation, we use the size of ideal chains, $R \approx bN^{1/2}$. On the time scale shorter than the Rouse time, a polymer undergoes structure reorganization and its center-of-mass shows sub-diffusive motion. On the time scale larger than the Rouse time, the polymer shows a normal diffusion. It is important to keep in mind that the Rouse diffusion coefficient and the Rouse time of a polymer are proportional to N^{-1} and N^2, respectively. Other interesting characteristics of the Rouse dynamics are summarized in Tab. 2.1

2.2.2 Reptation Model

As the length of the linear polymer elongated, its dynamic behavior is different from expected by the Rouse theory. The main reason of the discrepancy is its entangled structure (Fig. 2.9). Unlike short linear polymers, long ones are entangled to each other which prevents themselves from diffusing by the Rouse motion. Instead, entangled linear polymers are known to move through a mesh formed by other polymers. It can be also described by snake-like motion in a tube, so it is called reptation model.

In this model, a diffusion time is calculated by $\tau \approx L^2/D_{\mathrm{c}}$. Here, L is a contour length which is the length of the tube in Fig. 2.9, and D_{c} is a curvilinear diffusion coefficient, such that:

$$D_{\mathrm{c}} \approx \frac{k_{\mathrm{B}}T}{N\zeta}, \tag{2.36}$$

Figure 2.9 Schematic description of a reptation model. Dynamics of an long linear polymer (black) entangled with other polymers (gray) can be described by the motion of a snake.

which is the diffusion coefficient of the polymer along the direction of a tube axis. In order to calculate the self-diffusion coefficient and the diffusion time of the entangled linear polymer, we need to calculate the contour length, L. It is shown that the entangled linear polymer has an entanglement length N_e regardless of degree of polymerization N.[10] In other words, a polymer consists of blobs of size a corresponding to a tube diameter. This blob contains N_e monomers and its size also follows an ideal chain statistics, such that $a = bN_\mathrm{e}^{1/2}$. Because an entangled polymer has N/N_e blobs, the contour length is:

$$L \approx a\frac{N}{N_\mathrm{e}} \approx bN_\mathrm{e}^{1/2}\frac{N}{N_\mathrm{e}} \approx \frac{bN}{N_\mathrm{e}^{1/2}}. \tag{2.37}$$

Now, the time required for a polymer to escape from an old tube and to located in a new one which is called a disentanglement time is:

$$\tau \approx \frac{L^2}{D_\mathrm{c}} \approx \frac{\zeta b^2}{k_\mathrm{B}TN_\mathrm{e}}N^3, \tag{2.38}$$

Self-diffusion coefficient, in turn, can be calculated by:

$$D \approx \frac{R^2}{\tau} \approx \frac{k_{\mathrm{B}} T N_{\mathrm{e}}}{\zeta} N^{-2}, \tag{2.39}$$

which is scaled by N^{-2}. One can see that the diffusion coefficient of entangled linear polymers more rapidly decreases than that of unentangled linear polymers as N increases. Other interesting characteristics of entangled linear polymers are listed in Tab. 2.1.

Chapter 3

Structure of Ring Polymers

3.1 Introduction

Structures of non-concatenated, non-knotted rings in a melt has been intensively studied in recent years. While linear polymers in a melt show ideal statistics characterized by the Flory exponent $\nu = 1/2$ due to the screening of excluded volume,[4, 6] this argument no longer holds for the ring polymer. A number of numerical studies for ring polymer melts stated that the Flory exponent of a ring deviates from the that of an ideal chain, which varies from $\nu = 2/5$ to $1/3$.[11–21] Flory-type free energy minimization schemes done by Cates and Sakaue also supported the smaller Flory exponent than linear polymers.[22–24] It is interesting to note that, unlike the linear polymer case, the Flory exponent of a ring is not universal in all length scales of a ring size. Instead, as N increasese, it

varies from 1/2 corresponding to the ideal chain statistics to 1/3 corresponding to the compact globular structure. Recently, a noncrossing requirement leading to implicit constraints of non-concatenating and non-knotting is suspected as an origin of this distinguishable difference in the scaling relation between ring and linear polymer sizes. Nevertheless, the exact and universal theory for the ring polymer structure has not yet been provided rigorously. In this chapter, we review a theory for ring polymer structures, and present the molecular dynamics simulation results of a ring polymeric melt which is modeled by a bead-spring model.

This chapter is organized as follow. We first review the theory for estimating the size for ring polymers in a melt. Next, we explain the simulation method and the model that we used. The structural properties of a ring including size, looping probability and the coordination number of a ring polymer are discussed. We compare these results with the theory. Conclusion remark follows in the final section.

3.2 Theory

Here, we review the Flory-type mean-field free energy minimization to calculate the structure of a ring polymer in a melt, which is proposed by Sakaue.[23, 24] As mentioned above, a ring polymer have two topological constraints, non-concatenation and non-knotting constraints, due to the non-crossable bond (Fig. 3.1). While the non-concatenation constraint promotes the structure of the ring to be segregated, the ring can only shrink to a certain degree due to

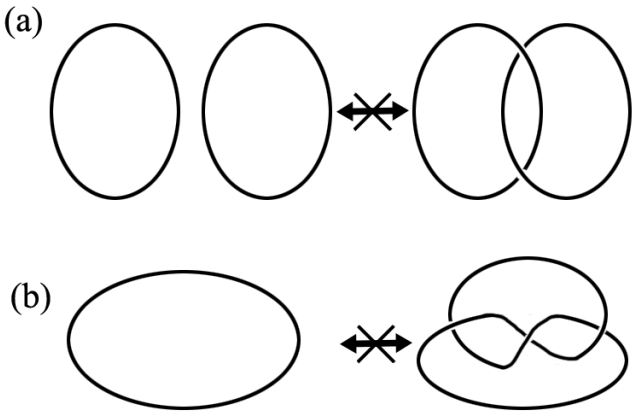

Figure 3.1 (a) Non-concatenation and (b) non-knotting constraints of a ring polymer. Because bonds can not cross each other, a ring imposes intrinsic constraints.

the requirement of a non-knotting constraint. In the original Flory argument for the linear polymer, an excluded volume interaction between monomers increases the free energy as shown in Eqn. 2.11. For the linear polymer melt, the effective excluded volume is screened out by other polymers, resulting in the ideal chain statistics. While the excluded volume of a ring would be screened out as well, two topological constraints dominate to determine the ring structure. In this theory, the two constraints are considered as an effective topological excluded volume to write down the free energy of a ring.

At first, the topological length scale can be defined in analogy to the entanglement length in the reptation model, a, in Eqn. 2.37. For the entangled linear polymer, a is independent of N as mentioned in Sec. 2.2.2. In contrast, the topological length scale for the ring polymer might depend on N, denoted

by $\xi_{\mathrm{R}}(N)$ which is supported by simulation studies.[15, 18] In turn, the number of monomers in a topological blob corresponding to the entanglement length N_{e} is, of course, dependent on degree of polymerization, which is denoted by $g_{\mathrm{R}}(N)$. Since the topology affects the structure on the length scale longer than the size of the topological blob, the subchain in the blob behaves like an ideal chain, which leads to $\xi_{\mathrm{R}}(N) \approx b g_{\mathrm{R}}(N)^2 \phi^{-1/8}$, where ϕ is a monomer volume fraction of the system.

Now, let us consider the ring polymer of the length N in a melt phase with the equilibrium size R. The number of neighboring molecules is approximately calculated by:

$$M_{\mathrm{R}} \approx \frac{R^3 \phi}{b^3 N}, \tag{3.1}$$

because $R^3\phi$ is a pervaded volume of a polymer and $b^3 N$ is an actual volume occupied a one polymer. Considering two rings interacting with each other through the effective topological interaction, one can define the effective topological excluded volume such that:

$$v_{\mathrm{R}} \approx R^3 Y, \tag{3.2}$$

where Y is the softening factor, which is independent of N. $Y = 1$ If the ring forms a perfectly circular morphology, and Y decreases to zero if other rings penetrate into the reference ring. Using these parameters, we define a new order parameter, a topological volume fraction, which contains information of the topological interactions of a ring, such that:

$$\phi_{\mathrm{R}} \equiv \frac{v_{\mathrm{R}} M_{\mathrm{R}}}{R^3} = M_{\mathrm{R}} Y. \tag{3.3}$$

Using this order parameter, we calculate the free energy of a topologically interacting ring. The first contribution to this free energy is originated from a non-concatenation constraint. A classical van der Waals fluid theory stated that the free energy density for a one component ideal fluid with an volume density ϕ and an excluded volume v is $f \approx -k_{\mathrm{B}}T(\phi/v)\ln(1-\phi)$.[5] Therefore, the non-concatenation effect for the free energy is expressed as:

$$\frac{F_{\mathrm{conc}}}{k_{\mathrm{B}}T} \approx -\ln(1-\phi_{\mathrm{R}}). \tag{3.4}$$

This equation indicates that a small value of ϕ_{R} leading to the segregates structure with the small ring size is favored due to the non-concatenation requirement.

The second contribution to the free energy of a ring is the non-knotting constraint. As the ring is confined in the cavity of a spatial size R due to the free energy of Eqn. 3.4, one can also write down the free energy cost for the confinement as:

$$\frac{F_{\mathrm{knot}}}{k_{\mathrm{B}}T} \approx \left(\frac{R_0}{R}\right)^{\delta} \approx \left(\frac{bN^{1/2}\phi^{-1/8}}{R}\right)^{\delta} \approx \left(\frac{NY^2\phi^{5/4}}{\phi_{\mathrm{R}}^2}\right)^{\delta/6}, \tag{3.5}$$

where $R_0 \approx aN^{1/2}\phi^{-1/8}$ is the size of an ideal chain. The last equality is obtained by using Eqs. 3.1 and 3.3. Under the requirement of an intensive free energy with respect to N, we obtain $\delta = 6$. Therefore, Eqn. 3.5 arrives at:

$$\frac{F_{\mathrm{knot}}}{k_{\mathrm{B}}T} \approx \phi_{\mathrm{R}}^{-2}NY^2\phi^{5/4}. \tag{3.6}$$

This non-knotting constraint, of course, contribute to have large value of ϕ_{R} in opposite direction to Eqn. 3.4.

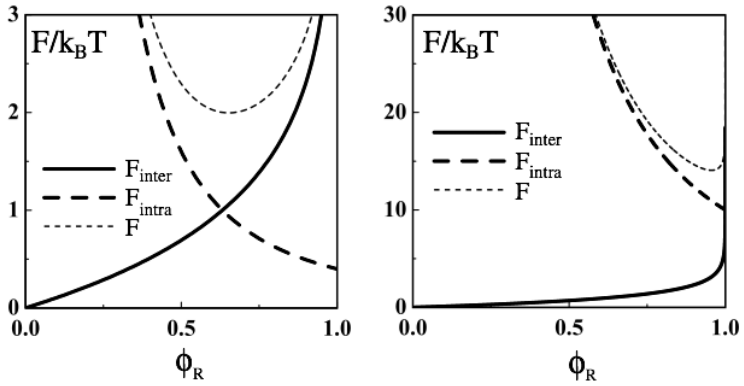

Figure 3.2 Free energy as a function of a topological volume fraction, ϕ_{R}, for (left) short and (right) long rings. This figure is cited from Ref. 23.

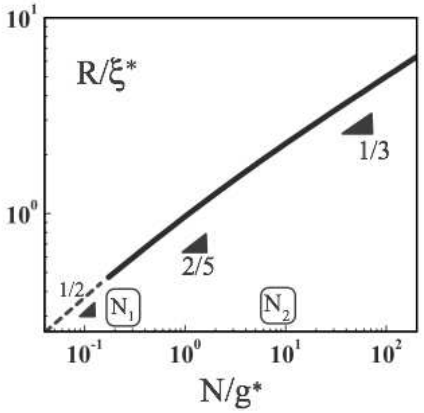

Figure 3.3 Size of a ring as a function of N obtained by numerical free energy minimization. g is an initial value of $N_{\mathrm{R}}(N)$ and $g^* \approx g/\phi_{\mathrm{R}}^{(\mathrm{eq})2}$. $\xi^* \approx \xi/\phi_{\mathrm{R}}^{(\mathrm{eq})}$ corresponds to the length scale of the second crossover, where ξ is the length scale of the subchain of g monomers. This figure is cited from Ref. 24.

Now, we minimize the total free energy, $F = F_{\text{conc}} + F_{\text{knot}}$, with respect to ϕ_{R}. Figure 3.2 shows the free energy as a function of a topological volume fraction, ϕ_{R}, for short and long rings obtained by numerical calculations. One can see that as the length of the ring increases, the topological volume fraction increases and converges to 1 at the asymptotic limit of $N \to \infty$. For the short ring (left in Fig. 3.2), one can calculate the softening factor Y and $\phi_{\text{R}} = \phi_{\text{R}}^{(\text{eq})}$ at equilibrium state. Calculated Y value allows one to minimize the free energy of a long ring with respect to N. Figure 3.3 shows the numerical results of the polymer size obtained by the free energy minimization as a function of N. It is interesting to note that there are two crossover lengths at which the ring structure statistics varies. For the short ring, while the size of a ring follows a ideal chain statistics characterized by the Flory exponent 1/2, the Flory exponent decreases to 2/5 for the intermediate rings. The second crossover points out the change of the ring structures from $\nu = 2/5$ to $\nu = 1/3$. The final expression of the ring size can be written as:

$$R \approx \xi_{\text{R}}(N)\left(\frac{N}{g_{\text{R}}(N)}\right)^{1/3}. \tag{3.7}$$

In this equation, both ξ_{R} and g_{R} are N dependent. ξ_{R} varies from ξ for the small ring to ξ^* for the long ring in Fig. 3.3. Simultaneously, g_{R} also grows from g to g^*. These two crossovers correspond to the two crossover lengths, N_1 and N_2 in Fig. 3.3. In asymptotic limit of $N \to \infty$, a ring forms a compact globular structure with the small flory exponent, $\nu = 1/3$.

The size of a ring in a melt is summarized as follows:

$$R(N) \sim \begin{cases} N^{1/2}, & \text{for } N < N_1 \\ N^{2/5}, & \text{for } N_1 < N < N_2 \\ N^{1/3}, & \text{for } N_2 < N. \end{cases} \tag{3.8}$$

3.3 Simulation Methods

Up to now, we showed two crossovers at which the ring structure varying from the ideal to the compact globular statistics. From now on, we show the molecular dynamics simulation results of a ring polymeric melt by comparing a linear counterpart. These results strongly support Sakaue's theory mentioned in the previous chapter.

In order to study static properties of linear and ring polymers in the bulk phase, we performed molecular dynamics simulations of polymers via the flexible Kremer-Grest model (Fig. 4.1).[10] In this model, a polymer consists of beads having unit mass m. Non-bonded beads interact with each other through repulsive Lennard-Jones (Weeks-Chandler-Anderson, WCA) potential (Eqn. 3.9) with the unit energy ϵ and the unit length σ. The covalent bond between beads is described by finite extensible nonlinear elastic (FENE) potential (Eqn. 3.10) to prevent bond crossing. Cosine angle potential is used to describe the stiffness of a polymer (Eqn. 3.11).

$$U_{\text{pair}}(r_{ij}) = \begin{cases} 4\epsilon[(\sigma/r_{ij})^{12} - (\sigma/r_{ij})^{6} + \frac{1}{4}], & r_{ij} < 2^{1/6}\sigma \\ 0, & \text{otherwise}, \end{cases} \tag{3.9}$$

$$U_{\text{bond}}(r_{ij}) = \begin{cases} -0.5kR_0^2 \ln[1-(r_{ij}/R_0)^2], & r_{ij} < R_0, \\ \infty, & \text{otherwise} \end{cases} \tag{3.10}$$

$$U_{\text{angle}}(\theta_i) = k_\theta[1-\cos(\theta_i - \pi)]. \tag{3.11}$$

In Eqn. 3.10, $k = 30\epsilon/\sigma^2$ and $R_0 = 1.5\sigma$ are used to suppress the bond length fluctuation. In Eqn. 3.11, $k_\theta = 1.5\epsilon$ .The unit time is scaled by $\tau = \sigma\sqrt{m/\epsilon}$. We employ the weak temperature coupling method, Langevin thermostat (Eqn. 3.12) in which a temperature, an integration time step, a friction coefficient are set to be $1.0\epsilon/k_{\text{B}}$, 0.01τ and $0.5\tau^{-1}$, respectively.

$$\ddot{\mathbf{r}}_i = \nabla \sum_{i \neq j} U_{ij} - \Gamma \dot{\mathbf{r}}_i + \mathbf{W}_i(t) \tag{3.12}$$

All simulations are conducted by GROMACS package.[25]

We simulate monodisperse polymer systems of six different lengths, $N =$ 16, 32, 64, 128, 256, and 512 for both linear and ring polymers (Tab. 3.1). The number density of monomers is $0.85\sigma^{-3}$, which is a typical monomer density of a melt for the bead-spring model. Obviously, periodic boundary condition is used to all directions. Concatenation and knotting dramatically change the properties of rings, but in this study, we focus on the properties of unlinked, unknotted ring polymers and such configurations are prepared as follows. At first, we place monomers with perfect circular morphology such that planes of the circles are perpendicular to z-axis. Centers of the circles are placed on square lattice sites in the xy-plane. To avoid concatenation between polymers, the lattice constant of the square lattice should be larger than diameter of fully

Table 3.1 System description: N, M, $L = L_x = L_y = L_z$, and t_{eq} are, respectively, the degree of polymerization, the number of polymers in a system, a system size, and an equilibration time. The monomer densities of all systems are $0.85\sigma^{-3}$.

N	M	L	t_{eq}
16	128	13.41	1.0×10^5
32	128	16.89	1.0×10^5
64	128	21.28	1.0×10^5
128	128	26.81	1.0×10^5
256	256	42.56	5.0×10^5
512	256	53.62	2.0×10^7

extended circles, so we set the lattice constant to $2.5r = 2.5N2^{1/6}\sigma/2\pi$, because $N2^{1/6}\sigma \approx 2\pi r$ for $N >> 1$, where r is radius of a circle. At high pressure of $P = 5.0\epsilon/k_{\mathrm{B}}$, short NPT simulations are performed until desired values of system size which satisfy $\rho = 0.85\sigma^{-3}$ are obtained. For all systems, desired densities are obtained within $5 \times 10^3\tau$. After equilibrating the systems during time larger than five times of Rouse time (Tab. 3.1), we perform production runs during $10^7\tau$.

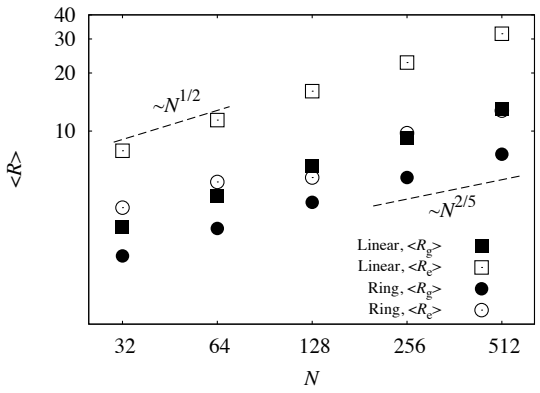

Figure 3.4 Gyration radii (open symbols) and end-to-end/spanning distances (filled symbols) of bulk linear (squares) and ring (circles) polymers as a function of N

3.4 Results and Discussion

3.4.1 Polymer Size

We first show the size of polymers as a function of N in Fig. 3.4 and Tab. 3.2. Radius of gyration R_{g} is defined by Eqn. 2.8 and the end-to-end distance for linear polymers and the spanning distance for ring polymers R_{e} are defined by:

$$R_{\mathrm{e}} = \begin{cases} |\mathbf{r}_1 - \mathbf{r}_N|, & \text{for linear polymers,} \\ |\mathbf{r}_i - \mathbf{r}_{i+N/2}|. & \text{for ring polymers.} \end{cases} \tag{3.13}$$

Figuere 3.4 shows that the size of linear polymer increases with $N^{1/2}$ as N increases. This power law is universal for all length scales. However, scaling behavior of the ring is, as expected from the theory, length dependent. While short rings follow ideal chain statistics, long rings have the smaller Flory exponent $\nu = 2/5$ than than short rings. Although our rings is not long enough

Table 3.2 Gyration radii and end-to-end distances (spanning distances) for linear and ring polymers in the bulk phase modeled by a bead-spring model.

	Linear		Ring	
N	R_g^2	R_e^2	R_g^2	R_e^2
16	4.71	29.19	2.51	8.48
32	10.22	62.54	5.09	16.10
64	21.42	129.94	9.80	29.73
128	43.46	250.06	18.27	33.01
256	85.10	513.13	33.01	95.21
512	170.24	1020.40	57.60	162.94

to reach an asymptotic of $\nu = 1/3$, we can see the first crossover between ideal chain and intermediate regimes.

It is also instructive to calculate the sizes of subchains. Figure 3.5 shows the sizes of subchains $R(s)$ as a function of a subchain length, s (contour length). Because both ends are connected to each other, the size of a subchain of a contour length $s < N/2$ is the same with a subchain of the length $(N - s)$. One can also find non-Gaussian statistics represented by $R(s) \sim s^{2/5}$ due to the connected chain end. In the asymptotic limit, it is expected that broad regime of $R(s) \sim s^{1/3}$ is observed.

3.4.2 Looping probability

One of interesting properties of a ring is looping probability, often called contact probability. One can define a loop as a structure of which two monomers

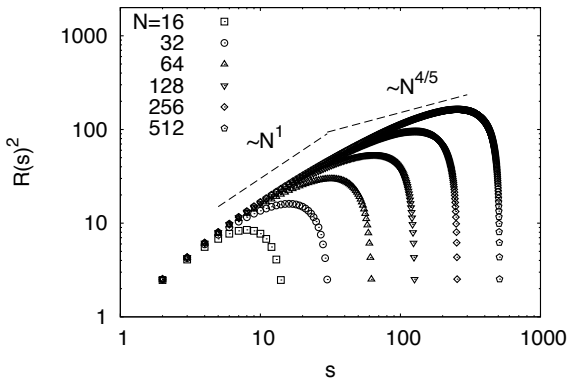

Figure 3.5 The sizes of subchains of the contour length s for ring polymers. Different symbols represent the different degree of polymerizations.Two dashed lines represent the scaling relations, $R(s) \sim s^{1/2}$ (left) and $R(s) \sim s^{2/5}$ (right)

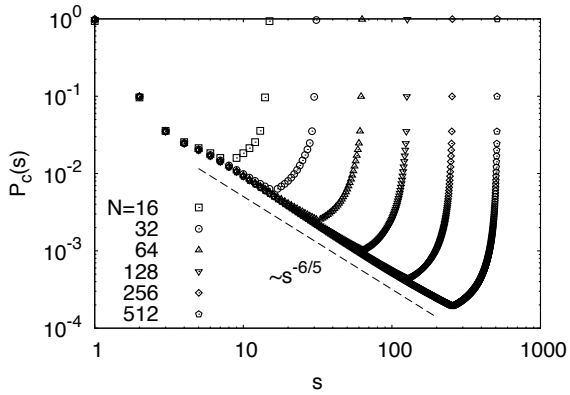

Figure 3.6 Looping probability of ring polymers as a function of contour lengths s. Different symbols represent the different degree of polymerizations. A dashed line represents the scaling relation $P_{\rm c}(s) \sim s^{-6/5}$.

separated by a contour distance s are contact with each other in space. This factor is very important especially in biological systems such as DNA packing problem.[26–28] Using the simulation trajectories, we calculate the looping probability as a function of s (Fig. 3.6). Here, we consider the two monomers being "*in contact*" when the distance between two monomers are closer than σ. It is well known that the looping probability follows a power law with respect to the contour length, such that $P_c(s) \sim s^{-\gamma}$. In Fig. 3.6, the looping probabilities for rings seem to be proportional to approximately $s^{-6/5}$ at $s < N/2$. This observation is different from that of linear polymers, $P_c(s) \sim N^{-3/2}$. The exponent γ for the looping probability of a polymer with the Flory exponent ν is simply calculated by mean-field approach.[18] The looping probability can be regarded as the probability of which the two end monomers of a subchain of the length s are located in the unit volume, σ^3. Therefore, it can be written as $P_c(s) \sim [\sigma/R(s)]^3 \sim s^{-3\nu}$. As a result, $\gamma = 3\nu$ which leads to $\gamma = 3/2$ for the linear polymer ($\nu = 1/2$) and $\gamma = 6/5$ for our rings ($\nu = 2/5$). In the asymptotic limit, slower decay of the looping probability with $P_c(s) \sim s^{-1}$ is expected. However, in order to avoid the convergence problem in calculating the total number of loops, $\int_0^N P_c(s)\mathrm{d}s$, γ should be larger than 1. A recent work showed that very long ring turns out to have this γ slightly above unity.[18].

3.4.3 Coordination Number

Finally, we show the number of contacting molecules for a ring polymer as a function of N by comparing with that for linear counterpart in Fig. 3.7. We consider the contacting molecular pairs for which at least one monomer pair

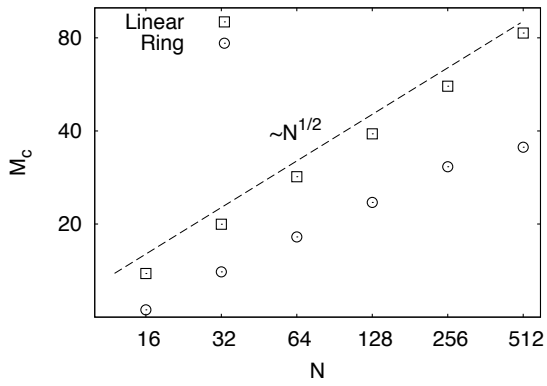

Figure 3.7 The numbers of contacting polymers per a molecule for linear (squares) and ring (circles) polymers as a function of N. A dashed line represents the scaling relation $M_{\rm c} \sim N^{1/2}$.

from each polymer are in contact to each other. We use the same definition of the monomer-monomer contact as in the previous section. This observable is usually called the coordination number of a polymer, and is approximately the same with the neighboring molecules $M_{\rm R}$ in Eqn. 3.1. In Fig. 3.7, one can readily find that $M_{\rm c}$ for linear polymers is proportional to $N^{1/2}$, which is proved in analogy to Eqn. 3.1. The linear polymer of the length N and the size R occupies a pervaded volume R^3 in space. Because the volume occupied by solely a single polymer is Nb^3, the number of polymers in this pervaded volume can be calculated by:

$$M_{\rm c}(N) \approx \frac{R^3\phi}{b^3 N} \sim N^{1/2}. \tag{3.14}$$

where the size of the linear polymer in a melt is expressed as $R \approx bN^{1/2}$. In contrast, the coordination numbers of rings seem to saturate at $N \to \infty$. It is well consistent with the theoretical estimation in Eqn.3.1. Combining with Eqs.

3.8, Eqn. 3.1 can be written as:

$$M_c(N) \sim \begin{cases} N^{1/2}, & \text{for } N < N_1 \\ N^{1/5}, & \text{for } N_1 < N < N_2 \\ N^0, & \text{for } N_2 < N, \end{cases} \tag{3.15}$$

which provides an evidence for the constant coordination number for the very long ring polymers.

3.5 Conclusion

Up to now, we have discussed the static properties of a ring polymer in a melt. Unlike a linear polymer melt which follows an ideal chain statistics, the statistics of a ring polymer structure in a melt varies with the degree of polymerization. This phenomenon is understood by following arguments: A ring polymer consists of topological blobs. On the smaller length scale than the size of this blob, the topology does not affect the structure of a ring. On the larger length scale, however, the topology effectively perturbs the ring structure from the ideal chain. Unfortunately, a size of the topological blob is not constant, instead, grows with N. It can be shown by the free energy minimization which is constructed by considering the two topological constraints as an effective excluded volume. As a result, two crossovers in the ring polymer size are observed and the very long ring adopts compact globular structure with the Flory exponent, $\nu = 1/3$. A series of thorough studies for the ring structure in a bulk as well as in a confined geometry would contribute to not only understanding the physics of biological circular macromolecules but finding new viscoelastic

materials. Based on this idea, we discuss how the confinement perturbs the structure of the ring polymer in a melt in the next chapter.

Chapter 4

Confinement Effect on Ring Polymers

4.1 Introduction

Understanding the nature of DNA packing during interphase in a nucleus for higher eukaryotes has been a long-lasting challenge in the field of biophysics. One of the most interesting features of DNA in a nucleus is chromosomal territories, in which chromatin fibers are not tangled to each other without making any knot, and each chromosome occupies a distinct territory.[29–31] Experiments have been performed to quantify the chromosome structure using, e.g., HiC for a contact probability [26–28] and FISH for subchain sizes.[32–34] In these works, the exponents of scaling relations for the contact probability $P_{\mathrm{c}}(s) \sim s^{-\gamma}$ and for the subchain size $r(s) \sim s^{\nu}$ versus the genomic distance s turned out

to be $\gamma \approx 1$ and $\nu \approx 1/3$, respectively. These experimental data provide both intriguing and challenging questions to polymer physicists since DNA, being a polymer with open ends, seems to provide different scaling exponents from those of entangled linear polymers characterized by $\gamma \approx 1.5$ and $\nu \approx 1/2$.[4, 6, 10]

An early theoretical suggestion to interpret the DNA packing in terms of polymer physics involves an idea of a crumpled globule. [35, 36] It is formed by a fast collapse of a single polymer as the solvent quality is quenched. Although the crumpled globule shares some characteristics with the chromosome, including knot-free configurations and the same fractal dimension, the idea still remains a hypothesis due to, e.g., long-term stability issue.[37] In recent years, inspired by aforementioned properties of crumpled globules, a ring in a melt has been proposed as a good candidate for elucidating the nature of DNA packing. [38, 39] Since both ends of the ring are connected to each other it possesses intrinsic topological constraints, non-knotting and non-concatenation, as represented in the chromosome structure.

Much attention has been paid to understanding of the effect of the topology of rings in a melt on their structures as mentioned in Sec. 3.1. In the early stage of these studies, it was understood that rings in a melt have an intermediate size characterized by the Flory exponent of 2/5 in a long length scale, which was supported by Flory-type argument[22] as well as simulation studies.[11–15] Recently, however, numerical simulations of sufficiently long rings gave an evidence for an asymptotic behavior of the ring size with the Flory exponent of 1/3 [17–21] as well as for the chromosome structures.[32–34] Especially, it turns out that a universal behavior of the ring sizes was found, regardless of

simulation models,[19] which provoked many theoretical studies regarding a better understanding of the ring statics. Modified Flory argument implementing topological constraints of the ring also reproduced the asymptotic behavior of the ring size and crossover behavior between an ideal and a compact polymer statistics.[23, 24] In these works, topological constraints are dealt with the effective excluded volume interactions. It is also fascinating that a simulation snapshot of ring polymers in a melt recently reported in Ref.8 allows one to recall the image of segregated chromosomes in a nucleus.[29] Motivated by the above works, showing knot-free, unentangled conformations similar to the interphase chromosome structures, study of the physics of rings in a melt has recently come into the spotlight.

Coming back to the problem of the DNA packing, it may be useful to review recent research activities focusing on the question why the chromatin fiber does not show reptation behavior even though it has free ends to reptate. One of the studies reveals that the reptation time of chromatin fiber is much longer than a cellular lifetime because its length is much larger than the nuclear size.[38] Bulky ends formed by repeated telomeric DNA sequence[40, 41] and some parts of chromatin fiber attached to inner surface of the nuclear envelope are also suspected to prevent the chromosome from relaxing to the intermixed state through reptation.[39] Along the line of these studies, it is worthwhile to investigate the adsorption of the DNA on the nuclear envelope in the language of polymer physics.

Much is known for the structures of confined linear polymer in a melt via experiments,[42–44] computer simulations,[44–47] and theories.[48–51] It is also

interesting to note that two-dimensional linear polymers in a melt, i.e., the limit of the ultrathin film, show highly segregated conformations and amoeba-like dynamics,[52–55] which resemble the physics of rings in a melt.[56] Compared to the linear case, a relatively little attention has been paid to the confined ring systems for the needs of understanding confined circular biopolymers, e.g., circular DNAs. Starting from the self-consistent field theory of a single adsorbed ring polymer on the surface,[57] some experiments[58–60], simulations[59, 61–63] and a theory[63] of confined ring polymers in a dilute regime have been performed. However, the confinement and the surfaces effects on the concentrated rings have remained a challenge. Problems in synthesizing the non-concatenated, non-knotted and monodisperse ring polymers make one difficult to investigate physics of confined rings in a melt by an experimental approach.[9]

In this study, therefore, employing molecular dynamics simulations, we study perturbation of confined ring structures by a surface and show how the surface affects the static properties of rings, e.g., ordering of local structures, sizes of rings, adsorbed amounts, and the coordination numbers of a polymer. The aim of this work is not only to investigate the ring structures when the surface effect is added to intrinsic topological constraints, but to look for new perspective for the nature of DNA packing in a nucleus.

The rest of this chapter is organized as follows. We first explain a flexible Kremer-Grest bead-spring model and a film system designed by implicit soft walls. After observing well-defined layering structures of monomers and bonds near the surface, we present structure perturbation on the scale of the polymer size. The static properties altered by the surface interaction and the topological

repulsion are also provided. Concluding remarks follow in the final section.

4.2 Simulation Methods

In order to study static properties of linear and ring polymers near the surface in a thin film morphology, we performed molecular dynamics simulations of polymers via the flexible Kremer-Grest model (Fig. 4.1).[10] In this model, a polymer consists of beads having unit mass m. Non-bonded beads interact with each other through repulsive Lennard-Jones (Weeks-Chandler-Anderson, WCA) potential (Eqn. 3.9) with the unit energy ϵ and the unit length σ. The covalent bond between beads is described by finite extensible nonlinear elastic (FENE) potential (Eqn. 3.10) to prevent bond crossing. No angle potential is included to describe flexible polymers. In Eqn. 3.10, $k = 30\epsilon/\sigma^2$ and $R_0 = 1.5\sigma$ are used to suppress the bond length fluctuation. Implicit soft walls perpendicular to z-axis are located at the bottom and top of z-axis. Two different non-bonded interaction potentials between the surface and a monomer are used to compare chain properties between attractive and repulsive surfaces. The attractive surface is represented by Lennard-Jones potential using the same parameters with WCA potential described above, except for the cutoff distance 2.5σ and attraction strength 3ϵ. The repulsive surface is modeled by WCA potential with the same parameter in the monomer-monomer repulsion. The unit time is scaled by $\tau = \sigma\sqrt{m/\epsilon}$. We employ the weak temperature coupling method, Langevin thermostat (Eqn. 3.12) in which a temperature, an integration time step, a friction coefficient are set to be $1.0\epsilon/k_{\mathrm{B}}$, 0.01τ and $0.5\tau^{-1}$, respectively.

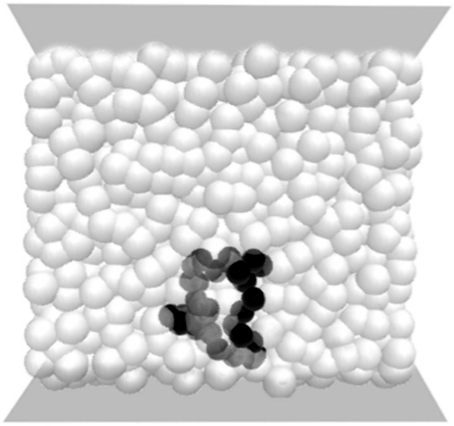

Figure 4.1 Schematic description of a simulation system of $N = 32$ ring polymers. A dark ring polymer represents one of adsorbed polymers.

All simulations are conducted by LAMMPS package.[64]

We simulate monodisperse polymer systems of five different lengths, $N =$ 32, 64, 128, 256, and 512 for both linear and ring polymers (Table 4.2). The number density of monomers is $0.85\sigma^{-3}$, which is a typical monomer density of a melt for the bead-spring model. To take into account the excluded volume of surfaces, we calculate the system volume by $V = L_x L_y L_z = L_x L_y (L_z^{'} - 2^{1/6}\sigma)$, where $L_z^{'}$ is the actual separation between two surfaces (Fig. 4.2). To avoid a bridged polymer, the separation between two surfaces should be larger than $4R_{\mathrm{g,bulk}}$, where $R_{\mathrm{g,bulk}}$ is the radius of gyration in the bulk phase. The bridging structure is not observed at all in our simulation trajectories. To minimize the finite size effect, we enlarge the system size along $x-$ and $y-$ directions and also increase the number of polymers in the system as N increases. Obviously, periodic boundary condition is used only in $x-$ and $y-$ directions (Table 4.2).

Table 4.1 System description: N, M, L_z, $L_x = L_y$, and $t_{\rm eq}$ are, respectively, the degree of polymerization, the number of polymers in a system, a film separation, a system size along x and y direction, and an equilibration time. The monomer densities of all systems are $0.85\sigma^{-3}$.

N	M	$L_z^{'}$	$L_x = L_y$	$t_{\rm eq}$
32	128	20.00	15.98	1.0×10^5
64	128	20.00	22.60	1.0×10^5
128	128	40.00	31.49	1.0×10^5
256	256	40.00	44.53	5.0×10^5
512	256	60.00	51.18	2.0×10^7

To focus on the properties of non-concatenated, non-knotted ring polymers we adopt the following preparation scheme. At first, after fixing the film separation to the desired value, we place monomers with perfect circular morphology and the planes of the circles are perpendicular to $z-$ axis. Centers of circles are placed on square lattice sites in the xy-plane. All monomers are located at the center between two surfaces. To avoid concatenation, the lattice constant of the square lattice should be larger than a diameter of a circle. To do so, we set the lattice constant to $2.5r = 2.5N2^{1/6}\sigma/2\pi$, because $N2^{1/6}\sigma \approx 2\pi r$ for $N >> 1$, where r is a radius of a circle. At high pressure of $P = 5.0\epsilon/k_{\rm B}$ in x- and y- directions, short NPT simulations are performed until desired values of L_x and L_y which satisfy $\rho = NM/L_zL_xL_y$ are obtained. In these preparation procedures, attractive interactions between chains are turned on by changing

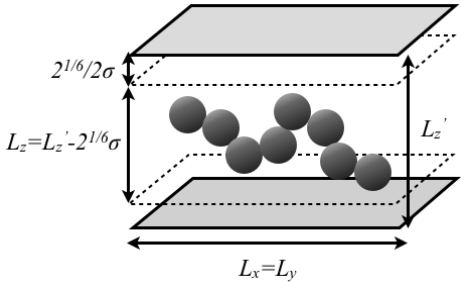

Figure 4.2 Schematic description of the surface-monomer excluded volume. It should be taken into account when one calculates the system volume.

the cutoff distance of WCA potential to $r_c = 2.5\sigma$. For all systems, desired densities are attained within $5 \times 10^3\tau$ (Table 4.2).

In order to equilibrate systems, NVT simulations are performed starting from the initial configuration obtained by the above method. We again change the cutoff distance of WCA potential from $r_c = 2.5\sigma$ to $r_c = 2^{1/6}\sigma$, to turn off intermonomer attractions. Equilibrations are executed during time larger than five times of Rouse time of polymers in the bulk phase. The lengths of production runs of all systems are $10^7\tau$ and the configurations are saved in every $10^2\tau$ to get ensemble averages.

4.3 Results and Discussion

4.3.1 Chain Non-ideality in the Vicinity of the Surface

Before studying properties of confined polymers, we first calculate the sizes of linear and ring polymers in the bulk phase as shown in Table 4.3.1. The density of monomers in the bulk is $0.85\sigma^{-3}$ as well as in the film system. As expected,

Table 4.2 Gyration radii and end-to-end distances (spanning distances) for linear and ring polymers in the bulk phase modeled by a flexible bead-spring model.

	Linear		Ring	
N	R_g^2	R_e^2	R_g^2	R_e^2
32	8.21	49.55	4.41	14.06
64	17.32	104.56	8.51	26.14
128	35.85	215.80	16.02	48.00
256	72.76	436.89	29.51	86.64
512	149.13	896.49	52.92	152.74

the fully flexible linear chains used in our simulation show ideal statistics characterized by the fractal dimension 2 (inset of Fig. 4.3). However, physics of ring polymers varies with the degree of polymerization N. Halverson et. al.[19] found striking merging behavior of the ring sizes for many different models, which provides a clear crossover from Gaussian regime represented by $R_g \sim N^{1/2}$ to compact globular regime by $R_g \sim N^{1/3}$ as shown in Fig. 4.3. Rings in this study correspond to $0.4N_e$ through $8N_e$ ($N_e \approx 70$ for the flexible bead-spring model [65]) and long rings of $N = 256$ and 512 lie on the intermediate regime in which the ring size is approximately proportional to $N^{2/5}$. They are expected to show the different physical properties from confined linear polymers due to the different Flory exponents.

Returning our attention to the confined polymers, it would be instructive to study the effect of local non-ideality in the vicinity of the surface induced by

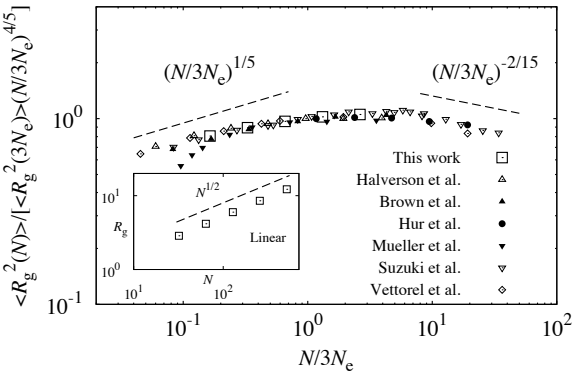

Figure 4.3 Rescaled gyration radii multiplied by $N^{4/5}$ of rings as a function of degree of polymerization normalized by entanglement length, N_e, which was originally provided in the work of Ref. 19. Those obtained in our simulations (black filled squares, $N_e = 70$) and other previous works in Ref. 11 ($N_e = 85$), Ref. 12 ($N_e = 40$), Ref. 18 ($N_e = 28$), Ref. 66 ($N_e = 140$), Ref. 67 ($N_e = 40$), and Ref. 68 ($N_e = 175$) are shown by different point types. Inset shows the gyration radii of our linear polymers, which are exactly scaled by $N^{1/2}$.

the excluded volume interaction between a monomer and a surface. We display variations of monomer densities, bond lengths, and bond alignments for linear and ring polymers as a function of the distance of a monomer from the surface z in Fig. 4.4. In this figure, it is shown that the oscillation of monomer densities fades away beyond $z \approx 4\sigma$ by forming four layers regardless of N. Results of $N = 512$ linear polymers within attractive surfaces are also plotted by black dotted lines in the same graphs. Linear and ring polymers with other N give almost the same variations with the $N = 512$ linear polymer (not provided here). The attractive surface leads to the polymer structure with more order, but the length scale hardly depends on the attraction strength. In the absence of a strong and long-range attraction such as Coulombic potential, the length scale of solely the excluded volume interaction between the monomer and the surface, usually $\approx \sigma$, is shorter than the polymer size. The surface contributes to forming the first layer whose thickness is about σ. The ordered monomers in the first layer help the monomers to be ordered in the second layer, and in turn, the third and fourth layers are also formed in a layer-by-layer fashion. During this procedure, ordering becomes weak as z increases. Such a layering structure is observed not only in polymer systems but in the various confined liquid systems, e.g., ionic liquids in the graphine double layers.[69]

Bond lengths and orientations are also oscillate near the surface. Second Legendre polynomial, $P_2(\cos(\theta))$, is calculated to obtain bond alignments by such that,

$$P_2(\cos(\theta)) = \frac{3}{2}\langle \cos^2(\theta) \rangle - \frac{1}{2}, \tag{4.1}$$

where θ is an angle between the bond vector and the normal to the surface.

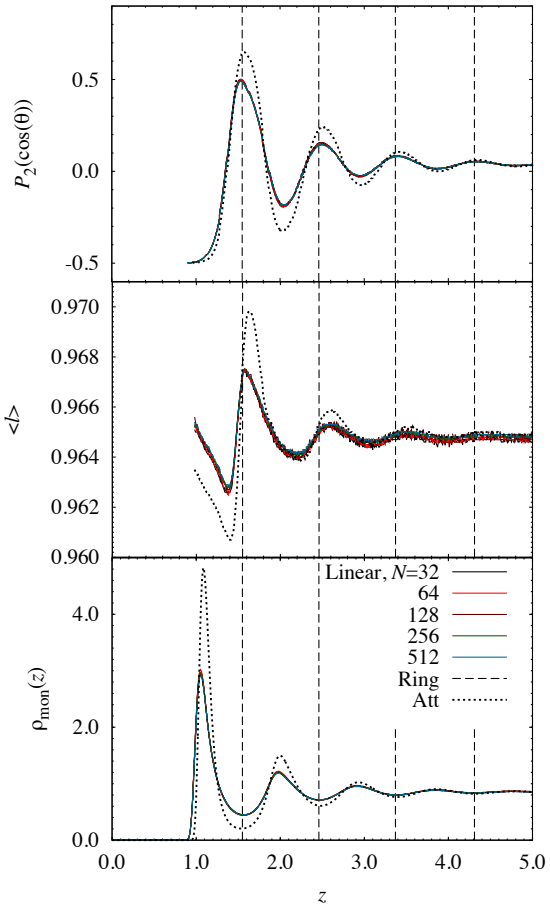

Figure 4.4 Variations of monomer densities (bottom), bond lengths (middle), and bond orientations (top) as a function of distance between the monomer and the surface. Black dashed lines represent the position at which densities of monomers are minimal. In all figures, results of attractive surfaces for linear polymers of $N = 512$ are represented by black dotted line.

This value varies from -0.5 meaning that the bonds are parallel, to 1.0 being perpendicular to the surface. When bonds align randomly, it is averaged out to be zero. Not only the monomer densities, bond lengths and alignments oscillate with the same amplitude and the wavelength regardless of N. In Fig. 4.4, black dashed vertical lines indicate the distances from the surface at which the monomer density is minimal. In the region where the monomers are sparsely distributed, the bonds are elongated and align perpendicular to the surface. In the dense region, in contrast, they contract and align with the surface. Note that only the magnitude of oscillation varies as the interaction strength between the surface and the monomer changes. These observations indicate that the bond length interaction hardly affects the structure ordering, and the oscillations of bond properties are chiefly determined by the monomer positions.

In addition to independence of the chain length and the surface attraction on the local structure ordering, the response of the confined polymer structure is insensitive to the chain topology (dashed lines in Fig. 4.4). The surface perturbs the polymer structures in a layer-by-layer fashion and the size of ring polymers is typically larger than the length scale of the surface-monomer excluded volume interaction. Thereby, the surface can not recognize whether the interacting monomers belong to the linear or the ring polymer. While an elongated layering structure is expected in the system of higher monomer density, all systems produce the same length scale of this non-ideal structure in our simulation condition regardless of the chain length, the strength of surface interaction and the chain topology. For the further discussion, it is useful to keep in mind that the length scale of the chain non-ideality, $\approx 4\sigma$, is even smaller than the sizes of

$N = 128 < 3N_e$ ring polymers giving ideal statistics characterized by the Flory exponent $\nu = 1/2$ (see Table 4.3.1 and Fig. 4.3).

4.3.2 Segment Properties

To study the effect of the surface-monomer interaction on the polymer structure, it is instructive to take into account the Silberberg hypothesis [70] based on the random walk with the reflective surface, which explains the physics of the confined linear polymer melts (Fig. 4.5). In this argument, assuming a reflecting boundary in the middle of an ideal chain, one can imagine that monomers which would have been located behind the boundary in the bulk phase are reflected through the boundary. Because of no excluded volume interaction between monomers in an ideal chain, the reflected monomers do not perturb the structure of remaining part of the chain, the consequence of which is that the parallel size of the chain does not vary from the bulk one.

The monomer excluded volume in the real system, however, cannot be screened out as argued in the structure ordering near the surface. Here we provide segment properties of adsorbed polymers, such as the sizes and the numbers of trains, loops and tails to understand the interplay between the chain non-ideality in the vicinity of the surface and the overall structure perturbation. The definitions of segments are the same as in previous works.[46, 50] As depicted in Fig. 4.6, successive adsorbed monomers are considered to a train, and the segment of successive non-adsorbed monomers whose both ends are adsorbed on the surface is a loop. A tail is defined by consecutive non-adsorbed monomers in both ends of a linear chain. Obviously, a ring polymer does not

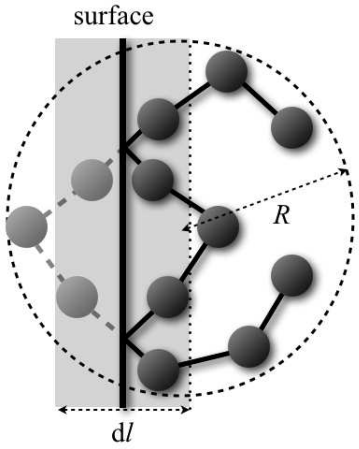

Figure 4.5 Schematic description (side view) of the conformation transfer through a reflecting boundary. Shaded monomers with orange color behind the surface are reflected in front of the surface. R is the polymer size if it were in the bulk phase and dl is the height of the disk represented by black shaded area.

have a tail. From now on, we discuss only the results of systems with the repulsive surface since the surface interaction strentgh modeled by short-range Lennard-Jones potential does not change structural properties of polymers significantly. Figure 4.7 presents the average numbers of loops $\langle n_{\rm l} \rangle$, trains $\langle n_{\rm tr} \rangle$, and tails $\langle n_{\rm tl} \rangle$ per an adsorbed chain as a function of N, where the adsorbed chain is defined such that at least one monomer belonging to it is located in the first layer represented in Fig. 4.4, which is identical to the definition in the Scheutjens-Fleer theory.[49, 50] In Fig. 4.1, the highlighted ring polymer is an example of an adsorbed chain. According to the definitions, the number of trains of a ring polymer is the same as that of loops if the perfectly adsorbed

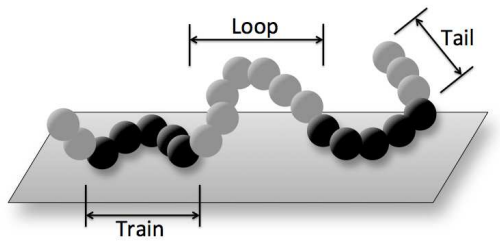

Figure 4.6 Schematic descriptions of a loop, a train, and a tail in a linear polymer. Monomers colored dark are adsorbed on the surface. Definitions of segments of a ring polymer are the same as those of a linear polymer.

polymer is absent. The relations, $n_{\rm tr} = n_{\rm l} + 1$ and $0 \leq n_{\rm tl} \leq 2$, also hold for linear polymers. In accordance with the recent work of Ref. 46, $\langle n_{\rm tr} \rangle$ and $\langle n_{\rm l} \rangle$ of linear polymers simultaneously grow with N, but $\langle n_{\rm tl} \rangle$ very slowly increases below 2. $\langle n_{\rm tr} \rangle$ and $\langle n_{\rm l} \rangle$ of ring polymers also increase with N, and are larger than those of linear ones. Figure 4.8 shows the average sizes of loops $\langle s_{\rm l} \rangle$, trains $\langle s_{\rm tr} \rangle$, and tails $\langle s_{\rm tl} \rangle$ per each segment. We find that $\langle n_{\rm tr} \rangle$ and $\langle s_{\rm tr} \rangle$ follow power laws as N varies with the scaling exponents, $\gamma_{\rm n}$ and $\gamma_{\rm s}$, respectively, such that $\langle n_{\rm tr} \rangle \sim N^{\gamma_{\rm n}}$ and $\langle s_{\rm tr} \rangle \sim N^{\gamma_{\rm s}}$ (Insets of Figs. 4.7 and 4.8). The fitted exponents for linear and ring polymers are listed in Tab. 4.3.2. It is intriguing to note that the sizes of trains for both linear and ring polymers, which slowly vary with N, are very similar to each other. The sizes of trains are determined only by the very local structure of polymers close to the surface. We argue that the length scale of structure ordering due to the surface is smaller than the that of chain ideality even of the ring polymers in a bulk phase. This indistinguishability between linear and ring polymer in a very short length scale leads to the same

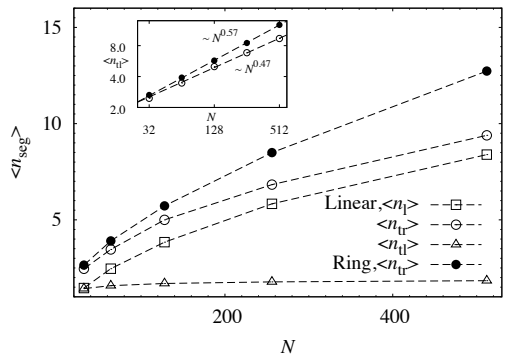

Figure 4.7 The average number and loops (squares), trains (circles), and tails (triangles) for linear (open symbols) and ring (filled symbols) polymers. Inset shows log-log plots of the number of trains. Average values can be scaled by N^{γ_n} and the fitted exponents are represented.

train size.

The probability distributions of segment sizes also support the above argument of the local indistinguishability between polymer topologies. Figure 4.9 and 4.10 display , repectively, the size distributions of trains and loops for $N = 512$ linear and ring polymers. As expected from the previous analytical[50, 51, 71] and numerical[46, 72] studies for the ideal chains, the train size distribution of linear polymers follows an exponential form, $P(s_{\rm tr})/\langle s_{\rm tr}\rangle \approx \exp(-s_{\rm tr}/\langle s_{\rm tr}\rangle)$, and the loop size distribution decays as a power law, $P(s_{\rm l}) \sim s^{-3/2}$, where s is a contour length. Notice that the train size distributions of linear and ring polymers are the same with each other, which means that the train size of the ring polymer melt can be explained in terms of ideal chain statistics. The fact that loop size distribution of the ring polymer is also similar with linear

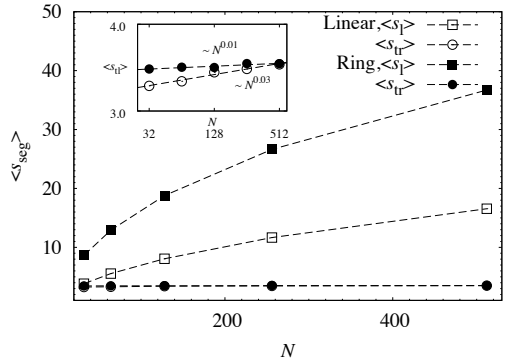

Figure 4.8 The average size of loops (squares), trains (circles), and tails (triangles) for linear (open) and ring (filled) polymers. The sizes of trains for linear polymers overlap with those for rings. Insets in both figures show log-log plots of the number and the size of trains. Average values can be scaled by N^{γ_s} and the fitted exponents are represented.

Table 4.3 Fitted scaling exponents for an adsorbed amount, δ, the average number of trains, γ_n, and the average size of trains, γ_s, versus N in the film and the bulk systems.

	Film		Bulk	
	Linear	Ring	Linear	Ring
δ	0.50	0.42	0.49	0.42
γ_n	0.47	0.57	0.48	0.58
γ_s	0.03	0.01	0.03	0.00

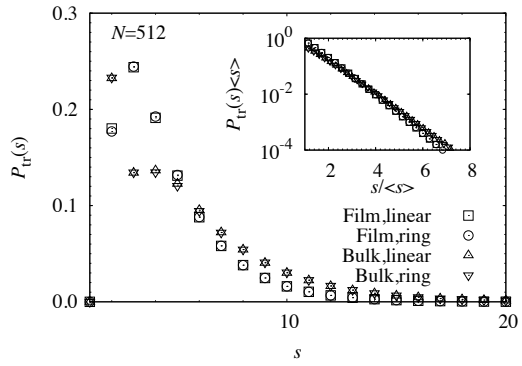

Figure 4.9 The probability distributions of train sizes for linear (squares) and ring (circles) polymers of $N = 512$. An inset is a log-linear plot of the train size distribution which shows exponential decay of probability distributions. Triangles and reverse triangles represent the distributions of train sizes for linear and ring polymers obtained in bulk system, respectively.

ones in small s also supports the argument of indistinguishability. Apparently, a high looping probability in large s of the ring polymer is originated from the topology of connected chain ends.

To explain the difference in the average numbers of segments between linear and ring polymers, we evaluate the segment properties of the bulk polymers in the following procedure. Based on the idea of random walk with the reflective boundary (Fig. 4.5), we place a fictitious slab parallel to the xy-plane and in the middle of $z-$axis of the simulation box whose thickness is two times of the layer thickness in Fig. 4.4, such that $\mathrm{d}l = 2 \times 1.05\sigma = 2.10\sigma$. We define a train in this system as successive monomers located in this slab, and a loop as successive monomers not located in the slab in analogy to the definition in the

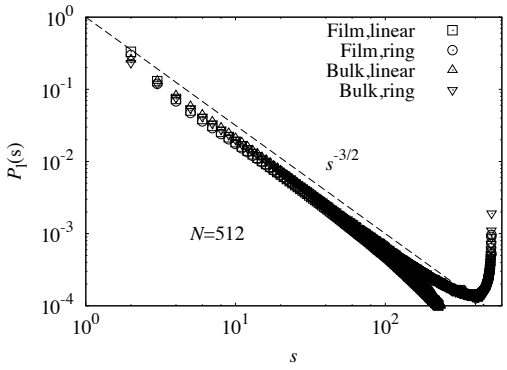

Figure 4.10 The probability distributions of loop sizes for linear (squares) and ring (circles) polymers of $N = 512$. Triangles and reverse triangles represent the distributions of train sizes for linear and ring polymers obtained in bulk system, respectively. All symbols seem to merge into a single line which is scaled by $P_l(s) \sim s^{-3/2}$ except for $s > N/2$ loops for rings.

film system. The size distributions of trains and loops of bulk polymers well reproduce the results of confined polymers in Figs. 4.9 and 4.10. The fact that fitted exponents of the relations $\langle n_{\rm tr} \rangle \sim N^{\gamma_{\rm n}}$ and $\langle s_{\rm tr} \rangle \sim N^{\gamma_{\rm s}}$ listed in Table 4.3.2 are also in agreement with those of confined polymers reveals the local ideality of a ring. Using the Silberberg's idea, the number of segments that visit the slab is regarded as the number of trains, which is closely related to the overall structure of polymer, especially, to the self-monomer density. The self-monomer density of a ring polymer in a melt is higher than that of a linear polymer.[18] Thereby the segments of the ring visit the slab frequently, resulting in the higher average number of trains.

4.3.3 Center of Mass Density

Up to now, we have focused on the local structure near the surface. The observation of the average numbers of trains motivates us to study the overall structure perturbation on the scale comparable to the polymer size. To do so, we first provide the density of polymer center-of-mass as a function of a distance of a polymer center-of-mass from the surface, z_{CM}, also normalized by the bulk radius of gyration, $R_{\mathrm{g,bulk}}$ (Fig. 4.11). Packing structure of polymer molecules toward the surface is observed as well as the monomer ordering. It is obvious that the size of polymers at $z_{\mathrm{CM}} < R_{\mathrm{g,bulk}}$ is influenced by the surface as represented by a red arrow in Fig. 4.11. One can find a noticeable difference between linear and ring polymers. Rings are more densly packed toward the surface than linear polymers reflected by the high peaks of the center-of-mass density profiles at $z \approx R_{\mathrm{g,bulk}}$. These high densities are compensated by the small densities at around $z \approx 2R_{\mathrm{g,bulk}}$. This trend resembles the packing of monomers which indicates that, unlike the linear polymers, the ring acts like a globular object rather than the ideal chain. It can be also understood by the topological excluded volume interaction imposed by the non-concatenation and the non-knotting constraints.[23, 24] Another observation of non-monotonous peak heights of rings at $z \approx R_{\mathrm{g,bulk}}$ with increasing N also supports this argument, which can be understood by two contributions of the local non-ideality and the topological repulsion. For small N, due to the comparable size of a ring to the length scale of the monomer packing structure, rings are densely packed. As N increases, the surface-induced non-ideal structure becomes a small part

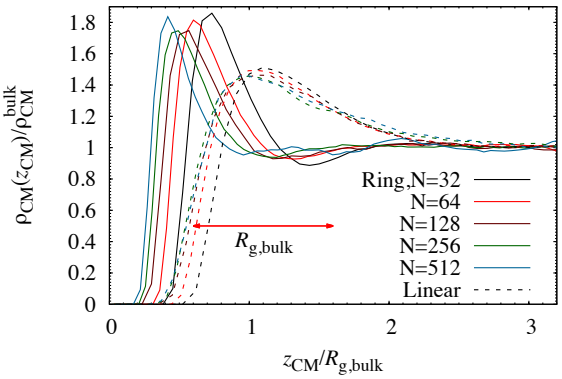

Figure 4.11 Densities of polymer center-of-mass normalized by the bulk density as a function of the distance from the surface also normalized by a radius of gyration of a bulk polymer for ring (solid) and linear (dashed) and polymers. A red arrow indicates the $R_{g,bulk}$.

of a ring, which weakens ordering of the molecules. If N continuously grows to the asymptotic regime ($\nu = 1/3$), the strong topological repulsion makes the ring again ordered.

4.3.4 Polymer Size Near the Surface

Motivated by the topological interaction of a ring on the large scale, we now study the non-ideality of a ring polymer on the scale comparable to its size. According to the above argument, a long ring of $N > 3N_e$ in a bulk is composed of ideal blobs of the size $\zeta \sim g^{1/2}$, where g is the number of monomers in this blob, expected to $g < 3N_e$. These blobs are densely packed with each other in space characterized by $R \approx \zeta(N/g)^{\nu} \sim N^{\nu}$, where $\nu = 2/5$ for long rings in this study. It is worthwhile to apply the ring to the argument of the conformation

transfer through the reflective boundary. Reflected blobs in front of the boundary experience topological interactions imposed by the non-knotting constraint, which makes the ring expand. In Fig. 4.12, we plot the gyration radii normalized by $R_{\mathrm{g,bulk}}$ versus $z_{\mathrm{CM}}/R_{\mathrm{g,bulk}}$. As the molecule approaches to the surface, it slightly shrinks at $z \approx R_{\mathrm{g,bulk}}$, but again swells in the vicinity of the surface for both linear and ring polymers. The increased amount near the surface is greater for ring polymers than that for linear counterparts. It is clear to see the parallel, $R_{\mathrm{g}}^{||}$, and perpendicular components, $R_{\mathrm{g}}^{\perp}$, of gyration radii to the surface as shown at the bottom of Fig. 4.12. $R_{\mathrm{g}}^{\perp}$'s for all systems merge into a single line within errorbars, which is in agreement with the above argument that the sizes of the polymers in $z_{\mathrm{CM}} < R_{\mathrm{g,bulk}}$ are affected. The validity of Silberberg hypothesis is underpinned by the obeservation that $R_{\mathrm{g}}^{||}$'s of the linear systems are not much deviated from their bulk sizes, in agreement with the previous work.[72] For this linear case, a slight expansion of chain sizes in the vicinity of the surface is due to the non-ideality by the surface-monomer excluded volume interaction whose scale is up to 4σ. For the ring polymer case, however, not only this short-range surface interaction but the topological repulsion enlarge the ring size along the parallel direction to the surface.

Figure 4.13 represents top-view snapshots of our simulations of $N = 128$ linear and ring polymers adsorbed on the surface. This figure clearly shows the difference of self-monomer densities of adsorbed polymers around their center-of-mass between linear and ring polymers. Linear polymers can penetrate into the space occupied by the other adsorbed linear polymer highlighted by dark color in Fig. 4.13 even at close to the surface. In contrast, a ring has hardly ever

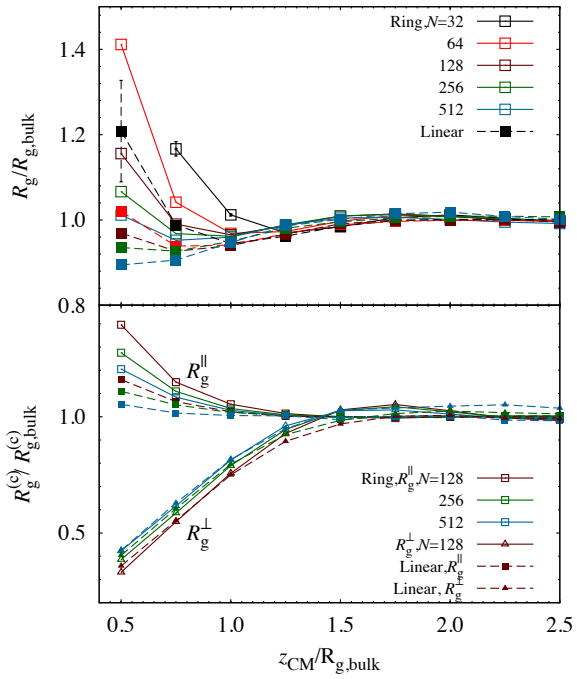

Figure 4.12 Normalized gyration radii (top) and their parallel and perpendicular components to the surface (bottom) as a function of the distance of a molecule center-of-mass from the surface, z_{CM}, for ring (open symbols) and linear (filled symbols) polymers. In the bottom, squares and triangles represent parallel and perpendicular sizes to the surface, respectively. In the upper figure, error bars for both polymers of $N = 32$ are shown. Errors in $z_{\mathrm{CM}}/R_{\mathrm{g,bulk}} \geq 0.75$ are smaller than the size of symbols.

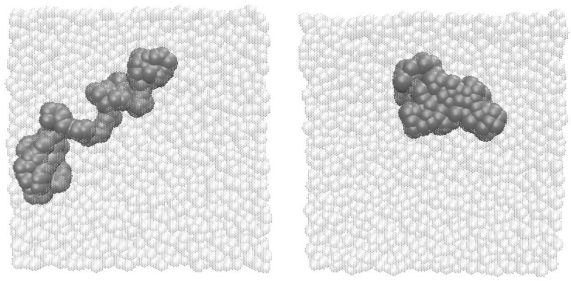

Figure 4.13 Top-view snapshots of $N = 128$ linear (left) and ring (right) polymers which are adsorbed on the surface. The surface interacting with highlighted polymers is located in front the page.

allows other rings to be tangled. Because of the topological excluded volume interaction, blobs in a ring repel each other, which causes the swelling of the ring under confinement.

4.3.5 Adsorbed Amount

We now present another physical property of confined polymers, an adsorbed amount Γ, whose behavior depends on the chain ideality and the topological interactions. We define Γ as the total mass of adsorbed chains per unit area. Figure 4.14 shows Γ as a function of N for both polymers. The adsorbed amount of a linear system increases with N with the power law, $\Gamma \sim N^{\delta}$, with the exponent $\delta_{\mathrm{l}} = 0.5$, which is well consistent with several previous studies. [46, 49, 50] One intriguing observation is a behavior of the adsorbed amount for the ring system. It also follows a power law, but the exponent is somewhat smaller than that of the linear polymer, $\delta_{\mathrm{r}} = 0.42$. Interestingly, these two exponents of linear and ring polymers seem to be close to their Flory exponents, ν_{l} and

ν_{r}, respectively. As pointed out earlier, a linear chain in a melt follows ideal statistics with $\nu_{\mathrm{l}} = 1/2$, but the sizes of $N = 256$ and 512 ring polymers lie on the intermediate regime with $\nu_{\mathrm{r}} \approx 2/5$ between an ideal chain and a compact globule (Fig. 4.3). In order to compare two exponents, ν and δ, we also plot the ratio of the adsorbed amount to the size, $\Gamma/R_{\mathrm{g,bulk}}$ as a function of N in the inset of Fig. 4.14. In this figure, the fact that the ratio is constant in asymptotic limit of $N \to \infty$ means that $\nu \approx \delta$. Using the picture of conformation transfer (Fig. 4.5), we can prove this relation for the linear polymer case via mean-field approach. The number of adsorbed monomers per a single adsorbed polymer, n_{ads}, can be evaluated by counting the number of monomers transpiercing the disk of the height $\mathrm{d}l$ and the radius R, which is described by shaded area in Fig. 4.5. Because the self monomer density, ρ_{self}, is proportional to N/R^3 and the volume of the disk is $V_{\mathrm{disk}} \sim R^2\mathrm{d}l$, the number of adsorbed monomers per an adsorbed polymer is calculated as:

$$n_{\mathrm{ads}} \approx V_{\mathrm{disk}} \times \rho_{\mathrm{self}} \approx R^2\mathrm{d}l \times \frac{N}{R^3} \sim \frac{N\mathrm{d}l}{R}. \tag{4.2}$$

If we let the size of the polymer in the bulk phase, R, be proportional to N^{ν}, then we can obtain $n_{\mathrm{ads}} \sim N/N^{\nu} \sim N^{1-\nu}$. Recall that each adsorbed monomer occupies almost the same area on the surface in Fig. 4.4 since the total number of monomers adsorbed on the surface, which corresponds to an area under the curve of the first peak, is regardless of N. From this, n_{ads} is proportional to the area occupied by an adsorbed polymer, and $1/n_{\mathrm{ads}}$ is proportional to the number of adsorbed polymers per unit area. The adsorbed amount, Γ, is the number of adsorbed polymers per unit area multiplied by the number of monomer in a

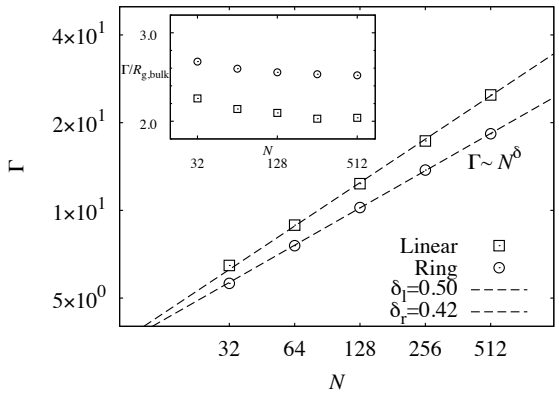

Figure 4.14 Log-log plots of adsorbed amounts, $\Gamma's$, as a function of N for linear (black) and ring (red) polymers. In both cases, adsorbed amounts are proportional to the N^{δ} and fitted exponents are expressed in legends. Inset shows the adsorbed amounts divided by gyration radii in the bulk, $\Gamma/R_{\mathrm{g,bulk}}$, versus N.

polymer, so finally, we can obtain that $\Gamma \sim N^{\delta} \sim n_{\mathrm{ads}}^{-1} \times N \sim N^{\nu}$, which reduces to $\nu = \delta$ for the ideal chain adsorbed on the reflecting surface. Discrepancy of two exponents at small N can be also explained by the comparable lengths between the local chain non-ideality and the polymer size.

It is an interesting problem to investigate why two exponents of ring polymers are similar to each other for large N even though they are not ideal. In Eqn. 4.2, we used the size of polymers in bulk phase, R, when calculating the volume of the disk and self-monomer density because they are considered as ideal chains. However, rings swell along parallel direction to the surface as observed in Fig. 4.12, thus we can not directly substitute the size of the adsorbed polymer into its bulk size in Eqn. 4.2. Instead, the volume of disk V_{disk}, is proportional

to $R_{\mathrm{g}}^{||2}\mathrm{d}l$ and the self-monomer density is proportional to $N/V_{\mathrm{ring}} \approx N/R_xR_yR_z$ where V_{ring} is the volume occupied by an adsorbed ring and R_α represents the gyration radius along α-direction ($\alpha = x,\ y,\ z$). Thereby, n_{ads} for the ring is:

$$n_{\mathrm{ads}} \approx V_{\mathrm{disk}} \times \frac{N}{V_{\mathrm{ring}}} \approx R^{||2}\mathrm{d}l \times \frac{N}{R_xR_yR_z}. \tag{4.3}$$

Figure 4.15 shows log-log plots of parallel size of linear and ring polymers versus N. In this figure, $R_{\mathrm{g}}^{||}$ seems to follow scaling behavior with exponent, ν', and fitted exponents for linear and ring polymers are 0.51 and 0.44, respectively. ν' of linear polymers is very close to the bulk one, $\nu = 0.5$, which is supported by the Silberberg hypothesis. However, it should be noted that the size of adsorbed ring polymers, even though their parallel sizes increase compared to those in the bulk as in Fig. 4.12, are scaled by the exponent which is very similar to Flory exponent. Especially, for long rings of $N = 256$ and 512, parallel polymer sizes are proportional to $N^{2/5}$, which yields the same scaling behavior as the bulk ring size. As a result, the scaling exponent of V_{disk} versus N does not change while we replace $R_{\mathrm{g}}^{||}$ by R in Eqn. 4.3.

It is also desirable to compare $R_{x,\mathrm{bulk}}^3$ ($\approx R^3$ in Eqn. 4.2) with $R_xR_yR_z$ for the valid substitution of the bulk self-monomer density into the adsorbed one, where $R_{x,\mathrm{bulk}}$ is radius of gyration along $x-$ direction of a bulk polymer. $R_xR_yR_z$ and $R_{x,\mathrm{bulk}}^3$ represent, approximately, V_{ring} in the film and in bulk phase, respectively. In Tab. 4.3.5, it is shown that the volume of a linear polymer adsorbed on the surface is much smaller than that in bulk phase because the parallel size is decoupled from the perpendicular one. The volume of an adsorbed ring polymer is, however, very similar with a bulk ring. This observation reflects

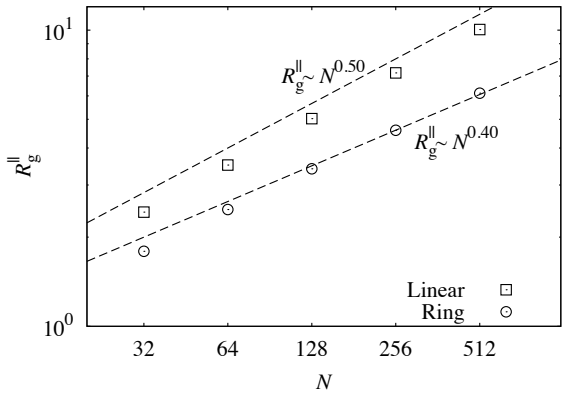

Figure 4.15 Log-log plots of parallel components of gyration radii to the surface versus N for linear (squares) and ring (circles) polymers. Two dashed lines represent $R_g^{||} \sim N^{0.50}$ and $\sim N^{0.40}$, respectively.

the highly packed structure of a ring because reduction of perpendicular ring size is compensated by increase of parallel size. The better consistency between R^3 and $R_x R_y R_z$ is expected for the more compact ring polymers of $N \to \infty$. According to this argument, by substituting R^3 into $R_x R_y R_z$, Eqn. 4.3 arrives at the same relation with the ideal chain (Eqn. 4.2) which reproduces $\nu \approx \delta$.

The exponent δ can be also obtained by the relation between the adsorbed amount and the train properties, using scaling exponents, $\gamma_{\rm n}$ and $\gamma_{\rm s}$. If there is no correlation between $n_{\rm tr}$ and s_{tr}, the product of two averaged qantities, $\langle n_{\rm tr} \rangle \times \langle s_{\rm tr} \rangle$ indicates the average number of adsorbed monomers per an adsorbed polymer, $n_{\rm ads}$. Because $1/n_{\rm ads}$ is proportional to the number of adsorbed polymers on unit area and $\Gamma/N \sim N^{\delta-1}$ as mentioned above, the equation, $1/n_{\rm ads} \sim N^{-\gamma_{\rm n}-\gamma_{\rm s}} \sim N^{\delta-1}$, arrives at $\delta = 1 - \gamma_{\rm n} - \gamma_{\rm s}$. Fitted scaling exponents

Table 4.4 Gyration radii in different directions and multiplication of three gyration radii in the film and bulk systems. Because gyration radii in different directions of a bulk polymer are almost the same, we use $R^3_{x,\mathrm{bulk}}$ instead of $R_{x,\mathrm{bulk}}R_{y,\mathrm{bulk}}R_{z,\mathrm{bulk}}$ in Eqn. 4.2.

	Linear			
N	R_x	R_z	$R_xR_yR_z$	$R^3_{x,\mathrm{bulk}}$
32	1.71	1.48	4.38	4.52
64	2.48	2.14	13.11	13.88
128	3.55	3.08	38.94	41.31
256	5.05	4.42	113.77	119.43
512	7.20	6.59	323.51	350.47
	Ring			
N	R_x	R_z	$R_xR_yR_z$	$R^3_{x,\mathrm{bulk}}$
32	1.27	1.10	1.76	1.78
64	1.75	1.53	4.71	4.78
128	2.40	2.11	12.22	12.35
256	3.25	2.86	30.10	30.85
512	4.34	3.81	71.76	73.09

of γ_n and γ_s with δ are listed in Table 4.3.2. Because the summation of three exponents equals unity, the number of trains and the size of train are uncorrelated. The relation, $\delta = 1 - \gamma_n - \gamma_s$, reflects that the dependence of N on the adsorbed amount is determined by those of train size and the number. γ_s for linear and ring polymers are almost the same with each other and are close to zero, which means that the effect of train size on the change of adsorbed amount is negligible. The main factor determining different adsorbed amounts between linear and ring polymers is the number of trains, which, in turn, is due to the difference in self-monomer densities.

4.3.6 Coordination Number

Another striking result in static properties of confined polymers is the decrease of the coordination number of a polymer, which is a good measure of conformational properties of polymeric melts. It is well known that while the coordination number of the linear polymer grows with $N^{1/2}$, that of the ring polymer saturates at $N \to \infty$ (inset of Fig. 4.16).[18] We evaluate the coordination numbers normalized by their bulk values as a function of z_{CM} in Fig. 4.16. Here, the number of contacting molecular pairs per a polymer is defined by the coordination number, where two polymers of which at least one monomer-monomer pair is closer in space than σ are regarded as the contacting pair. Note that the amount of decrease for the ring is larger than that for the linear counterpart except for the $N = 32$ case. This observation reveals that the repulsive topological interaction due to the reflecting blobs makes the locally tangled neighboring rings squeeze out. From this result, it is strongly suspected that

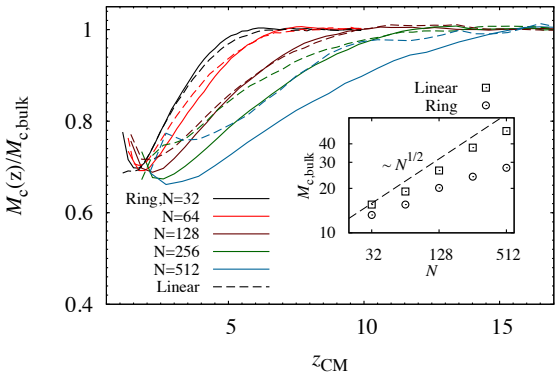

Figure 4.16 Coordination numbers normalized by bulk values for ring (solid lines) and linear (dashed lines) polymers as a function of the distance of the polymer center-of-mass from the surface. Different colors represent different lengths of polymers. An inset shows the coordination numbers of linear and ring polymers in bulk phases.

the confinement effect contributes to forming a segregated chromosome in a nucleus. For $N = 32$ linear case, the small chain size comparable to the non-ideality in the vicinity of the surface leads to the exceptional drop of the number of surrounding molecules.

4.4 Conclusions

In this work, we have presented structures of confined ring polymers in a melt by comparing those of ideal chains. Ring polymers in a melt are known to form compact structure by packing ideal blobs. The length scale of local structure ordering due to the surface-monomer excluded volume interaction is shorter than

the size of the ideal blob, which leads to the very similar local structures between linear and ring polymers. According to the Silberberg's reflecting boundary argument, the reflecting blobs of linear polymers do not feel the excluded volume interaction. In contrast, reflecting parts of ring polymers feel the repulsion with other blobs due to the topological excluded volume interactions. As a result, the confined ring crowds out the neighboring molecules which makes itself more compact, and it expands along parallel direction to the surface. Because we have yet to reach very long rings in asymptotic limit, the exponents obtained in this work, ν, δ, $\gamma_{\rm n}$, and $\gamma_{\rm s}$ are not universal. Nevertheless, we found interesting relations between these exponents which are expected to also hold for very long rings due to the stronger topological effect than our rings. Moreover, longer rings are expected to show the larger amount of parallel size expansion and a bigger drop of the coordination number than our ring polymers. Our observations provide the possibility that segregated conformation of chromosomes is originated from the confinement effect in a nucleus envelope in addition to the factors mentioned in the introduction, e.g., a long disentanglement time of a chromatin fiber and a telomeric region at the end. In this view point, it is challenging to investigate variation of crossover lengths of the ring polymer structure from ideal to globular statistics under the confinement. In addition to the confinement effect, various aspects for the interplay between the physics of ring polymer melt and the chromosome packing are currently under study.

Chapter 5

Dynamics of Ring Polymers

5.1 Introduction

Rheological properties of polymeric materials have been of great interest to many researchers in recent years. In general, polymers show different dynamical behaviors with their inherent topologies. For example, linear and branched polymers show different dynamical scaling behaviors.[4, 6] Recently, ring polymers have brought about novel issues to the dynamics in polymeric melt phase. Their crumpled globular structures with high fractal dimensions on a sufficiently large length scale resemble several biological molecules, existing as chromosomal territories in cells.[8, 18, 39, 59, 67, 73] One of the interesting dynamical features is the diffusion behavior of unknotted, unlinked ring polymers. A few years ago, Kawaguchi and coworkers succeeded in synthesizing highly

mono-disperse ring polymers,[74, 75] and found that the diffusive motion of ring polymer melts rapidly slows down as the degree of polymerization, N, increases. In this case, it was found that the diffusion coefficient shows a scaling behavior as $D \sim N^{-1.9}$. A number of simulation studies also reported similar scaling relations of the diffusion coefficient with its scaling exponent ranging from -2.4 to -1.9.[12, 14, 56, 66] Interestingly, it turns out that these values are very similar to those found in the reptation model of linear polymer melts, although topological constraints in ring polymers do not allow them to move around as in the reptation model. It is also noteworthy that the scaling relations are consistent with a few theoretical works based on the lattice animal model of the double-stranded conformation of the rings.[22, 76] However, a plateau modulus that is characteristics of entangled polymer melts, and systematic double- stranded configurations have not been observed in the ring polymer simulations.[56] These observations present intriguing questions regarding the nature of diffusive behaviors in the ring polymer melts.

A couple of simulation studies have provided some clues to the mechanism of diffusive motions in ring polymer melts. One of them is decoupled time scales between diffusion and structure reorganization.[56] This decoupling behavior has not been observed in entangled linear polymers, whose scaling exponent of the disentanglement time versus N, which turns out to be 3, is exactly the same as that of the structure relaxation time.[10] The fact that the ring polymer diffusion time is much larger and more rapidly increases with N than the internal structure relaxation time has been used as an evidence to support the idea of amoeba-like motion of ring globules.[54, 56]

It is fair to say that neither the simulation nor the theory has succeeded in suggesting a clear mechanism of ring polymer dynamics yet. One of the difficulties in simulation studies is defining a threading configuration in the melt phase. One of the most well established and generally applied analysis methods in revealing entanglement effects is primitive path analysis (PPA) pioneered by Kremer and coworkers.[65, 77] In linear polymer melts, the PPA can provide the shortest path of polymers by fixing positions of both end monomers, and can reveal the entanglement effect between different chains, which then allows one to calculate the entanglement length and the plateau modulus. Halverson et al. applied PPA to ring polymers by fixing two opposite particles randomly, and clearly demonstrated entangled rings, although they were not able to identify clearly the effects of entanglement on the dynamics.[56] We also note in passing that Michieletto et al.[21, 78] studied slowing down of the ring polymers in a pre- constructed gel structure. Although these works do not give direct evidence for the threading effect on the dynamics of ring polymer melts, it provides an intriguing question for the threading effect on the ring polymer dynamics.

In this work, we provide an alternative measure for calculating the threading time, that is, statistical distributions of so-called persistence and exchange times of molecular contacts in polymer melts. The distributions of persistence and exchange times and their decoupling behaviors have been originally developed in the study of dynamical heterogeneity observed in glassy systems, and have been used very successfully as a measure to characterize fluctuation-dominated dynamics in supercooled systems and ionic liquid systems.[79–82] We utilize this new method to study how threading affects dynamical slow-down of ring

polymer diffusions by studying statistical distributions of persistence times in molecular contacts.

This chapter is organized as follows. In Simulation method section, we first briefly explain the model and the simulation methods. We provide a definition of threading time, and show how the threading motions affect the dynamical behavior of ring polymers. Comparisons between ring threading with linear entanglement also provide molecular evidences for elucidating slow-down of ring polymer dynamics. Concluding remarks follow in the final section.

5.2 Simulation Method

We perform molecular dynamics simulations using a bead-spring model developed by Kremer and Grest[10] as well as in Sec. 3.3. In this model, potential energy functions for non-bonded interactions, bond stretchings, and angle bendings are represented by Weeks-Chandler-Andersen (WCA) (Eqn. 3.9), Finite-Extensible-Nonlinear-Elastic (FENE) (Eqn. 3.10), and cosine angle potentials (Eqn. 3.11), respectively. A weak temperature coupling method is applied to the system using the Langevin thermostat (Eqn. 3.12). We simulate linear and ring polymer systems for various cases with different number of monomers in a polymer, N = 16, 32, 64, 128, 256, and 512. All systems consist of 128 monodisperse polymer molecules and the number density of monomers is set to be 0.85. All preparation procedures are the same with Sec. 3.3. While the entanglement length of linear polymers for this model is known as $N_{\mathrm{e,linear}} \approx 28$,[65] that of a ring has not been well-established yet. The recent numerical study

reported $N_{e,ring} \approx 77$ for rings, by counting the number of monomers in a Kuhn segment of the primitive path in analogy to the linear polymer,[56] but interplay between Ne,ring and the ring dynamics still remains unclear. Although our longest ring does not reach an asymptotic scaling regime in their sizes,[19] its length is much longer than N_e,ring and it has a value of Flory exponent, $\nu = 2/5$, which is smaller than that of short rings and linear polymers. Thus it is expected that our long rings are long enough to study threading effects in ring polymers. After equilibrating the system during time longer than three times of the Rouse time,[6, 83] we perform production runs until the mean square displacement of polymer's center-of-mass motion reaches a diffusive regime.

As a control system, we also perform simulation studies of diffusional motions of spherical particles, which mimic the dynamics of a very compact globular ring polymer without a threading effect. The radius of the sphere is chosen such that the radius of gyration and the mass of the sphere are the same as those of a polymer. We set the volume fraction to be the same with the polymer system. The other simulation parameters are the same as those of polymer systems. GROMACS package is used in all equilibration and production runs.[25]

5.3 Results and Discussions

5.3.1 Definition of Threading Dynamics

A typical threading configuration between two rings is shown in Fig. 5.1 in terms of a schematic representation and in Fig. 5.2 which is a simulation snapshot for $N = 128$ ring system. In Fig. 5.1, the threaded ring (gray) cannot diffuse or

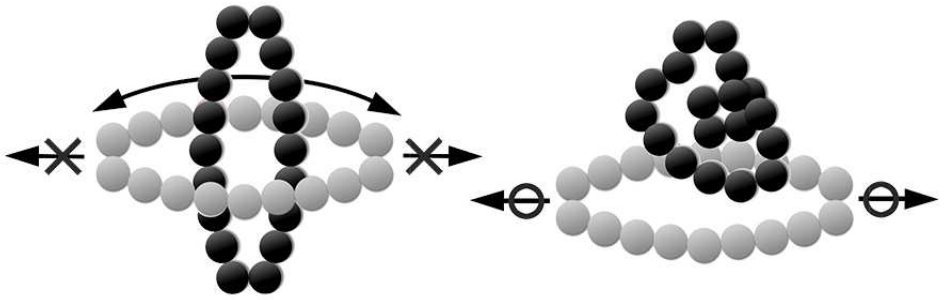

Figure 5.1 Schematic descriptions of threading dynamics. A gray ring represents a threading polymer, and a black ring is a threaded polymer.

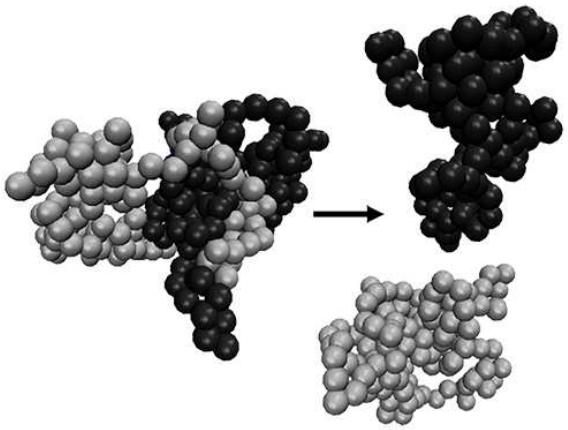

Figure 5.2 Simulation snapshot of $N = 128$ rings for explaining the threading dynamics. A gray ring represents a threading polymer, and a black ring is a threaded polymer.

diffuse together with the treading ring as long as the threading configuration is maintained. When the threading ring (black) unthreads as in the right of Fig.5.1, the threaded one can finally diffuse away. This picture is also illustrated

by simulation snapshots shown in Fig.5.2, where a gray ring forming a large loop is threaded by a black polymer. These figures illustrate the basic idea of threading dynamics of ring polymers, that is, why rings diffuse so slowly even through there is no entanglement effect.

5.3.2 Decoupling of Structure Relaxation and Diffusion

One of the important observations in threading dynamics is that diffusion time and structure relaxation time of ring polymers are decoupled, unlike those of linear chains. In simulation studies of polymers, a different types of the mean square displacements (MSDs) are calculated,

$$g_1(t) = \langle [\mathbf{r}_i(t) - \mathbf{r}_i(0)]^2 \rangle \tag{5.1}$$

$$g_2(t) = \langle [\mathbf{r}_i(t) - \mathbf{r}_{\mathrm{CM}}(t) - \mathbf{r}_i(0) + \mathbf{r}_{\mathrm{CM}}(0)]^2 \rangle \tag{5.2}$$

$$g_3(t) = \langle [\mathbf{r}_{\mathrm{CM}}(t) - \mathbf{r}_{\mathrm{CM}}(0)]^2 \rangle \tag{5.3}$$

Here, $\mathbf{r}_i$ and $\mathbf{r}_{\mathrm{CM}}$ are the positions of a monomer and a center of mass, respectively. $g_1(t)$ is the ensemble average of the monomer displacement and $g_3(t)$ is that of the center-of-mass displacement. $g_2(t)$ is a kind of time-correlation function of the distance between a monomer and the center-of-mass, which starts from 0 at $t = 0$ and converges to $\langle R_{\mathrm{g}}^2 \rangle$ at long time. Figure 5.3 shows MSDs of $N = 128$ linear and ring polymer melts, and Fig. 5.4 displays the MSDs of center of mass for linear and ring polymers. At long time, all the systems except for $N = 512$ linear polymers reach diffusive regime, at which $g_3(t)$ is proportional to t^1. We obtain diffusion coefficients, D_{G}, by fitting the diffusive regime of $g_3(t)$ to the equation $g_3(t) = 6D_{\mathrm{G}}t$.

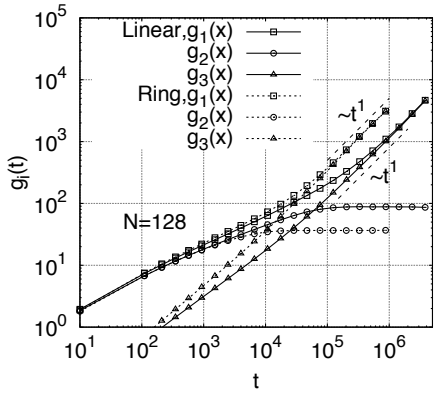

Figure 5.3 $g_1(t)$, $g_2(t)$, and $g_3(t)$ for $N = 128$ linear (solid lines) and ring (dashed lines) polymers.

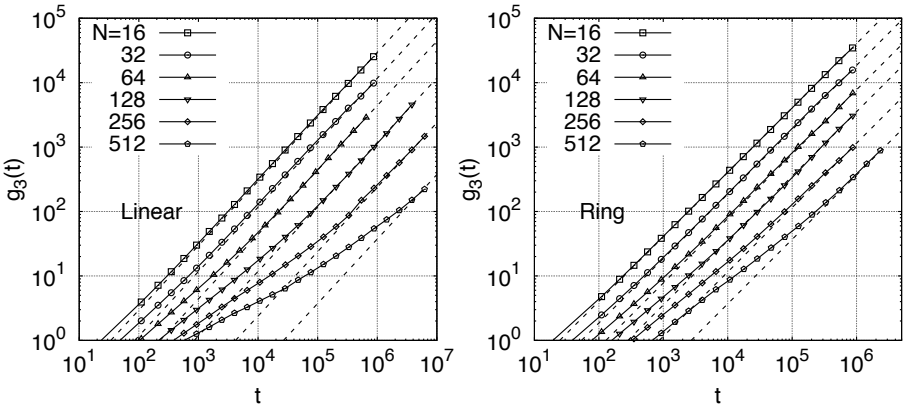

Figure 5.4 Mean square displacements of center of mass ($g_3(t)$) for linear (left) and ring polymers (right) in melts.

Time-correlation functions of the end-to-end vectors for the linear polymers, and spanning vectors for the ring polymers are used to calculate the structure

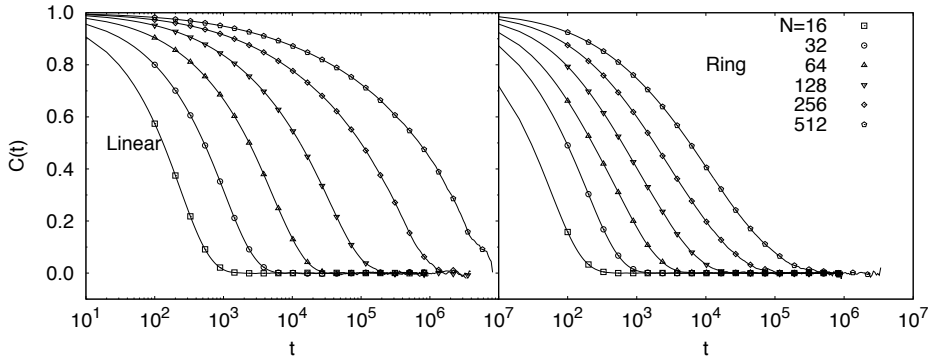

Figure 5.5 time correlation functions of linear (left) and ring polymers (right). Different polymer lengths are depicted in different colors.

relaxation times, where

$$\mathbf{r}_{\mathrm{ee}}(t) = \begin{cases} \mathbf{r}_1(t) - \mathbf{r}_N(t), & \text{for linear polymers,} \\ \mathbf{r}_i(t) - \mathbf{r}_{i+N/2}(t), & \text{for ring polymers.} \end{cases} \tag{5.4}$$

More precisely, when calculating the positions of i-th monomer in a ring polymer, we average the positions of five adjacent monomers from $(i-2)$-th to $(i+2)$-th monomers. Figure 5.5 shows the time-correlation function of the linear and ring polymers, and they show stretched exponential behaviors. We can obtain the structure relaxation times by integrating the correlation function from 0 to infinity.

Figure 5.6 shows the diffusion and structure relaxation times of linear and ring polymers. This figure clearly shows that, in the linear polymer case, both time scales are almost the same, and they are scaled by $\sim N^3$. However, in the ring polymer case, not only the absolute values of diffusion times but the scaling exponent versus N are much larger than those of structure relaxation

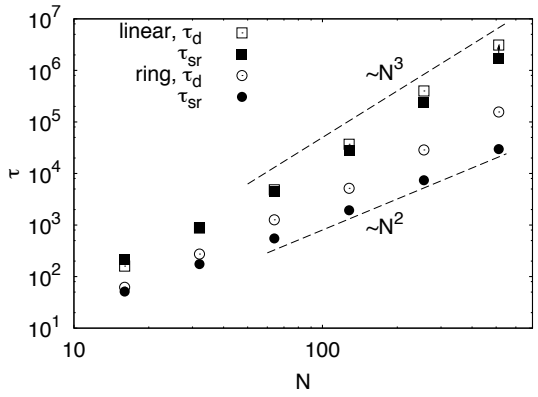

Figure 5.6 Diffusion time (open, $\tau_{\rm d}$) and structure relaxation times(filled, $\tau_{\rm sr}$) of linear(squares) and ring(circles) polymers.

times, which means that the rings reorganize their internal structures before they move around about the distance corresponding to their sizes. This result is also consistent with the previous study of Halverson et. al., which shows the decoupling of diffusion coefficients and friction coefficients for ring polymer melts.[56] Fast memory loss of spanning vectors is mainly caused by spinning motions of rings around the specific axis formed by the threading polymer without diffusion (Fig.5.1), which can be a good evidence for threading dynamics of ring polymers.

5.3.3 Definition of Persistence and Exchange Times

For analyzing entangled configurations, the PPA method has been used for linear polymer melts.[65, 77] However, it is not straightforward to extend the method to the ring polymer melts. The PPA may also be likely to miss some of the threading configurations for ring polymers when randomly picked two

monomers of a threading polymer are located along the same direction from the needle plane formed by a loop of the threaded polymer. Therefore, in this paper, we propose an alternative method for obtaining statistics of threading times based on persistence time distributions of molecular contacts. Persistence times and related exchange times were first proposed by Jung et al.[79] as a good measure to identify dynamically heterogeneous behavior of glassy systems. In glass forming liquids that are typically modeled by atomistic Lennard-Jones liquids or kinetically constrained lattice models, mobile and immobile regions of the system are identified and labelled with a binary variable, n_i. Usually, the binary variable is assigned 1 or 0, whether it corresponds to a mobile or immobile region, respectively. In such coarse-grained models, persistence time, τ_{p} is defined by the time duration over which a mobile (or an immobile) region persists from $t = 0$ until $t = \tau_p$, where the state of the mobility changes. A related, but different statistical measure is called an exchange time, τ_x, as a time duration between two mobility-changing (or exchange) events at time t and time $t + \tau_x$.[79] For stochastic model systems, it is known that there is an exact relation between probability distributions of persistence ($P_{\mathrm{p}}(t)$) and exchange times ($P_{\mathrm{x}}(t)$), such that[79]

$$P_{\mathrm{p}}(t) = \frac{\int_t^\infty dt' P_{\mathrm{x}}(t')}{< \tau_{\mathrm{x}} >} \tag{5.5}$$

where $\langle \tau_{\mathrm{x}} \rangle = \int_0^\infty \mathrm{d}t P_{\mathrm{x}}(t) t$ is a mean exchange time. Moreover, for Poisson processes where exchange events are not correlated to each other, two probability distributions are identical to each other and they have exponential decay forms in time. However, when there are strong correlations between the exchange

events, the two distributions decouple from each other.

To adjust this idea to polymer systems, we characterized molecular contact between two polymers as a binary variable. To do so, we first define $s(i, j; t)$ as a binary, contact variable, which takes 1 when the centers of mass of the i-th and j-th polymers are separated less than the sum of their radii of gyrations at time t, and 0 otherwise,

$$s(i,j;t) = \begin{cases} 1, & \text{if } |\mathbf{r}_{\mathrm{CM},i}(t) - \mathbf{r}_{\mathrm{CM},j}(t)| < R_{\mathrm{g},i}(t) + R_{\mathrm{g},j}(t), \\ 0, & \text{otherwise,} \end{cases} \tag{5.6}$$

where $\mathbf{r}_{\mathrm{CM},i}(t)$ and $R_{\mathrm{g},i}(t)$ are the center of mass position and the radius of gyration of i-th polymers at time t, respectively. If one ring threads another, those two rings are expected to be in a contact with each other. Therefore, using the contact variable, we can study dynamical behavior of the threading events by calculating probability distributions of persistence and exchange times for contact pairs. Since threading configurations only contribute to the contact pairs, we count persistence and exchange times for the contact pairs only.

5.3.4 Contact Lifetimes for Polymeric Systems

We first tested this method by applying the idea to a simple system consisting of spherical particles. In this case we used the radius of the sphere when calculating contact variables in Eqn. 5.6. Figure 5.7 shows probability distributions of persistence and exchange times of spherical system corresponding $N = 32$ ring polymers. In the case of spherical particles, one can see that the probability distributions of persistence and exchange times are exponential and identical to each other as shown in Fig.5.7 and its inset. This indicates that the dynamics

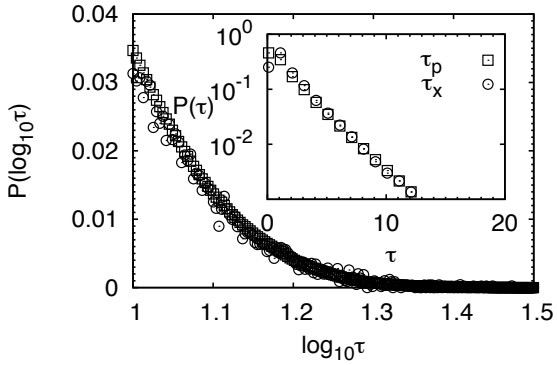

Figure 5.7 Probability distribution of persistence (squares, $\tau_{\rm p}$) and exchange time (circles, $\tau_{\rm x}$) distributions, which is represented by $P(\log_{10}\tau)$ versus $\log_{10}\tau$. Inset shows a linear-log plot of the same distribution which shows exponential decay of the distributions.

of spherical particles is completely Poissonian, caused by random diffusional motions.

In polymeric systems, however, there are two different time scales that contribute to statistics of persistence and exchange time distributions. The first one is random diffusion which is characterized by an exponential distribution at short time as in the simple sphere system. The more important and interesting one is long persistence and exchange times shown as long tails in the distributions of Fig.5.8. Because of this long tail, two distributions of polymer systems are decoupled from each other especially for long polymers. According to the relation between persistence and exchange times given in Eqn.5.5, higher probability of finding longer exchange times results in fat tails in the distribution of persistence times at larger values. It is an intriguing question

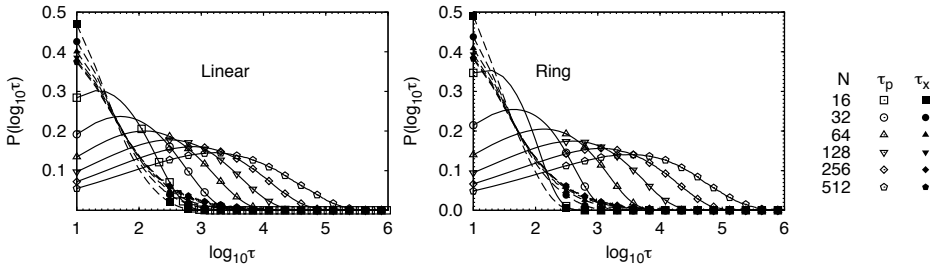

Figure 5.8 Probability distribution of persistence (open symbols, $\tau_{\rm p}$) and exchange time (filled symbols, $\tau_{\rm x}$) distributions for linear (left) and ring (right) polymers represented by $P(\log_{10}\tau)$ versus $\log_{10}\tau$.

to ask what mainly contributes to long persistence and exchange times. As mentioned before, we expect that if one ring is threaded by another ring, a contact is formed between them. For linear polymers, molecular contacts are well captured by entanglement effects, because one polymer is confined in loops formed by another polymer. For ring polymers, however, diffusional motions of the threaded ring is restricted due to the threading ring, which prevents them from separating out. Therefore, we expect that the threading dynamics of ring polymer melts is mainly responsible for long exchange and persistence times.

Following the idea presented above, we calculated distributions of threading times. Fig.5.9 shows linear-log plots of persistence and exchange time distributions (open squares and circles, respectively) for $N = 512$ ring polymers. In a very short time, the probability distributions decay almost exponentially as shown by the linear plots in log-linear scales. Since this short time part is due to the diffusion of non-threading polymers, not threading dynamics, we subtract

this part from the original distributions after fitting the short time distribution to an exponential function, $P_{\text{short}}(t) = c_{\text{s}} \cdot \exp(-t/\tau_{\text{s}})$, and then renormalize the distributions (Tab.5.1). The resulting distributions of threading times are shown as filled squares and circles in Fig.5.10, and they look similar to each other. In the case of linear polymers, it takes some time, called disentanglement time, for an entangled polymer to escape from the previous confining tube and to be located in a new tube. This disentanglement time is closely related to threading time which it takes for two threaded polymers to separate out. Therefore, as in the case of entangled linear polymers, a threaded ring polymer also needs unthreading time to escape from threading configuration. The fact that threading time of ring polymer is related to disentanglement time of linear polymers makes it possible to anticipate threading effect on ring polymer dynamics.

5.3.5 Average Threading Times

Lastly, to quantitatively compare the threading times of linear and ring polymers, we obtained average persistence and exchange times for threading configurations. In Fig.5.11, it is shown that, for polymers of $N < 64$, both threading times of ring polymers are smaller than those of linear ones, but for long polymers of $N > 128$, threading times of rings dominate over those of linear polymers. Here, errors of the average times can be estimated by those of contact persistence and exchange times listed in the Tab.5.2, in which the standard errors(SE) are about four orders of magnitude smaller than its average values for all systems. Since we use only short time data set when fitting distributions, errors caused by the fitting procedure are also negligible as shown in Fig.5.9.

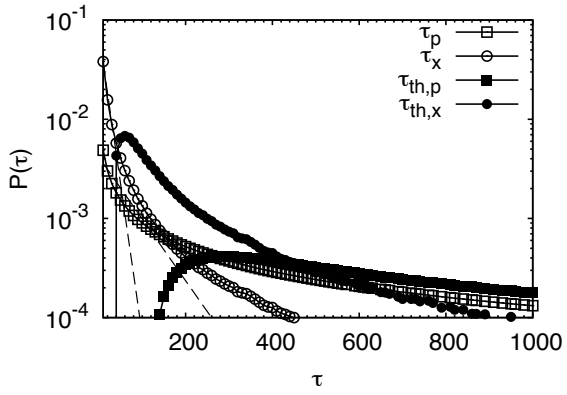

Figure 5.9 Linear-log plot of probability distributions of persistence (open square, $\tau_{\rm p}$) and exchange time (open circle, $\tau_{\rm x}$) distributions for $N = 512$ ring polymers. Threading persistence (filled squares) and exchange time (filled circles) distributions obtained by subtracting short time contributions are also shown. Dashed lines represent fitted function of short time contribution, $P_{\rm short}(t)$. See the main text for more details.

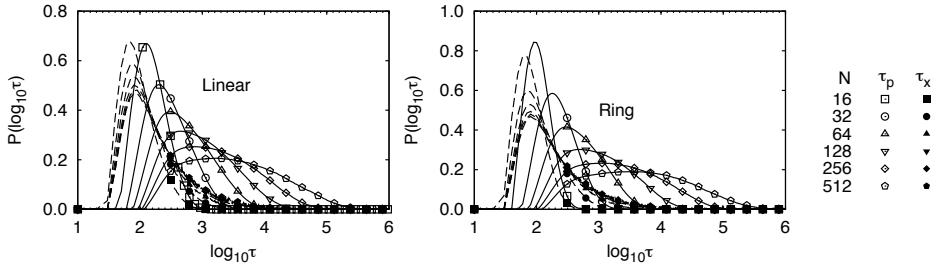

Figure 5.10 Probability distribution of threading persistence (open symbols, $\tau_{\rm p}$) and exchange time (filled symbols, $\tau_{\rm x}$) distributions for linear (left) and ring (right) polymers represented by $P(\log_{10}\tau)$ versus $\log_{10}\tau$.

Table 5.1 Short time fitting parameters of persistence and exchange time distributions to the function, $P_{\mathrm{short}}(t)$. Subscripts, 'p' and 'x' mean the parameters corresponding to the persistence and exchange time distributions respectively.

	Linear				Ring			
N	$c_{\mathrm{s,p}}$	$\tau_{\mathrm{s,p}}$	$c_{\mathrm{s,x}}$	$\tau_{\mathrm{s,x}}$	$c_{\mathrm{s,p}}$	$\tau_{\mathrm{s,p}}$	$c_{\mathrm{s,x}}$	$\tau_{\mathrm{s,x}}$
16	0.369	24.594	1.016	12.617	0.531	20.937	1.097	12.183
32	0.225	34.560	0.863	13.685	0.259	32.406	0.914	13.174
64	0.140	45.273	0.784	14.285	0.146	44.090	0.821	13.731
128	0.092	56.149	0.743	14.582	0.090	54.927	0.779	14.101
256	0.047	65.179	0.723	14.709	0.059	63.918	0.756	14.260
512	0.047	71.530	0.716	14.710	0.042	72.677	0.750	14.263

Therefore, we expect that the standard errors of the average threading times are much smaller than the symbol size in Fig.5.11. Interestingly, the crossover length between $N = 64$ and 128 turns out to be similar with the entanglement length of ring polymers, $N_{\mathrm{e,ring}} = 77$, as revealed in a previous study using PPA.[56] It is also interesting to note that the crossover length scale is related to the universal behavior of polymer sizes. According to a number of previous researches studying ring polymer sizes,[18, 23, 36, 67] Flory exponent decreases from 1/2 to 1/3 depending on degree of polymerization. The crossovers between different scaling regimes are universal, independent of ring polymers simulated by different models.[19] The first crossover from $\nu = 1/2$ to 2/5 is at $N \approx 3N_{\mathrm{e,linear}}$ and the second from 2/5 to 1/3 is at $N \approx 30N_{\mathrm{e,linear}}$,

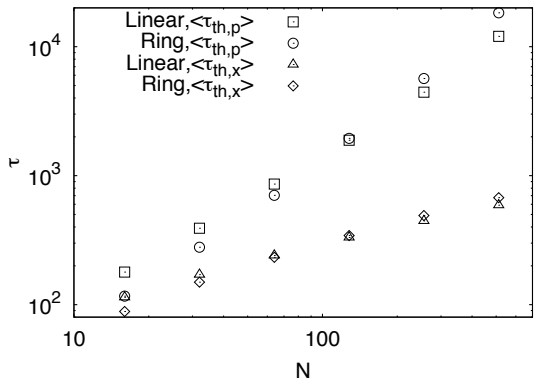

Figure 5.11 Average threading persistence and exchange times of linear and ring polymers. The sizes of error bars for all systems are much smaller than the size of symbols.

which is a characteristic feature of ring polymer melts. However, linear polymer melts have a Flory exponent of 1/2, regardless of the degree of polymerization.

From a theoretical point of view, threading time is closely related to the self-excluded monomer volume. For a crumpled globule, it is well known that a relatively small fraction of inner volume of a ring polymer is penetrated by surrounding polymers.[18] This small self- excluded volume contributes to the threading dynamics in two different ways. The first contribution comes from the reduced inter-ring overlap which leads to a small threading probability. The second is, in contrast, that an elongated contour length of the threaded primitive path increases threading times. In analogy to the reptation model of entangled linear polymer melts, the threading polymer squeezes through the loops of surrounding threaded polymers. The squeezing time which is regarded as a threading time is proportional to the contour length of the primitive chain

Table 5.2 Averages and standard errors of the contact persistence and exchange times.

	Linear			
N	$< \tau_{\mathrm{p}} >$	SE($< \tau_{\mathrm{p}} >$)	$< \tau_{\mathrm{x}} >$	SE($< \tau_{\mathrm{x}} >$)
16	6.5139×10^{0}	1.7052×10^{-3}	3.5189×10^{0}	6.5941×10^{-4}
32	1.6563×10^{1}	2.8035×10^{-3}	5.2092×10^{0}	1.1642×10^{-3}
64	4.2377×10^{1}	7.0837×10^{-3}	7.4175×10^{0}	1.9826×10^{-3}
128	1.1012×10^{2}	1.7916×10^{-2}	1.0335×10^{1}	3.3756×10^{-3}
256	2.8450×10^{2}	3.8029×10^{-2}	1.3853×10^{1}	4.8201×10^{-3}
512	8.5024×10^{3}	3.7516×10^{-1}	1.8303×10^{2}	9.2414×10^{-3}
	Ring			
N	$< \tau_{\mathrm{p}} >$	SE($< \tau_{\mathrm{p}} >$)	$< \tau_{\mathrm{x}} >$	SE($< \tau_{\mathrm{x}} >$)
16	4.0350×10^{0}	8.4147×10^{-4}	2.8836×10^{0}	6.5449×10^{-4}
32	1.1291×10^{1}	2.5664×10^{-3}	4.6585×10^{0}	1.3615×10^{-3}
64	3.4681×10^{1}	8.2982×10^{-3}	7.1503×10^{0}	2.7674×10^{-3}
128	1.1434×10^{2}	2.8169×10^{-2}	1.0542×10^{1}	5.6263×10^{-3}
256	3.8270×10^{2}	9.8045×10^{-2}	1.4973×10^{1}	1.1315×10^{-2}
512	1.3563×10^{4}	3.3556×10^{-1}	2.0485×10^{2}	1.8805×10^{-2}

for the threaded polymer, and this contour length is also monotonically increases when the inner space for surrounding rings to interpenetrate diminishes. Our observation on the threading times indicates that the latter effect is a dominant one in determining an average threading time. Even though the long ring in a melt has a low probability of threading, once the threading is made, a ring

spends much time to unthread, which results in the slowing down of the ring dynamics. The fact that the degree of polymerization at the first crossover is approximately the same with our crossover length of average threading times between linear and ring polymers strongly supports this argument. The polymer length corresponding to the second crossover, $N \approx 840$, is out of range in our simulation studies. However, we expect that more compact globular rings with a small self-excluded monomer volume exhibit very long threading times, which provides a major contribution to the slowing down of ring polymer dynamics.

5.4 Conclusion

In this work, we show that threading and unthreading events are important factors in determining dynamics of ring polymers by using persistence and exchange times of polymer contacts. As opposed to linear polymer melts, Flory exponent of ring polymer melts decreases from 1/2 to 1/3 as degree of polymerization increases. Since the small Flory exponent of polymers leads a high looping probability, ring polymer melts are more probable to form the threading configurations than linear polymer melts. If one ring threads another, diffusion of the threaded ring is restricted and the overall diffusion of ring polymer melts slows down. Slow diffusion of the threaded ring is represented by a fat tail in the exchange time distribution of molecular contacts, resulting in decoupled persistence and exchange time distributions. The degree of polymerization at which the threading time becomes important is consistent both with the entanglement length of ring polymers, and the crossover length of Flory exponent.

In spite of the successful analysis of the threading effect of ring polymers presented above, we note that the average threading times are about ten times smaller than the structure relaxation times and diffusion times. The exponent in scaling behavior of average threading time versus degree of polymerization, that is $\tau_{\mathrm{th,p}} \sim N^2$ in Fig.5.11, is also somewhat smaller compared to diffusion time. It may be the case that there are some threading configurations that our definition of molecular contact can not capture. For example, threading configurations of two small loops sticking out of their main bodies of which the distance between their centers of mass is longer than the sum of their radii of gyrations is not recognized by the contact. To understand the effects of the missing threading configurations on the overall distribution of persistence and exchange time distributions, a more precise definition of threading configurations may be necessary. It is also desirable to develop analytical theory of treating threading configurations using static properties of polymers, including looping probability, contact probability between molecules, and the size of subchain to help further understanding of threading dynamics of longer ring systems that are not easily studied by molecular dynamics simulations. Various aspects of threading dynamics along these lines are currently under study.

Chapter 6

Concluding Remarks

In this thesis, we have discussed the structures and dynamics of a ring polymeric melt. While linear polymeric melts which are deeply understood and widely applied in various research fields, the ring polymer physics just has begun to emerge. Especially, biological importances such as the circular macromolecules and the segregated chromosomes in a eukaryotic nucleus provide motivations to study the ring polymers. Therefore, using the theoretical and numerical approaches, we present several interesting properties of ring polymers. Considering that most of biological molecules are confined in specific geometries, we study confinement effect on the structure of ring polymeric melts. This study shows that the ring becomes compact and segregated under confinement. Although rings in our simulations are not long enough to show the asymptotic behavior, it is shown that some scaling exponents which are closely related to the

Flory exponent may characterize the topological class of polymer. Simulations for longer ring as a future work would be helpful to prove our arguments.

Moreover, we also study the origin of slow dynamics of a ring polymer. Unlike the entangled linear polymer, a mathematical definition of the threaded ring configuration is not well established yet, thus it is not easy to provide a direct evidence for the threading dynamics. In this thesis, therefore, we show slowing down of the ring polymer dynamics caused by the threading in terms of the decoupling of persistence and exchange time distributions. We are also interested in the structure and dynamics of two-dimensional ring polymer melts. In addition to two topological constraints of a ring polymer, two-dimensional rings intrinsically possesses a non-threading constraint. Therefore, understanding the physics of two-dimensional ring polymer melts would be helpful for elucidating the ring polymer physics in three dimension. All these studies for the structure and dynamics of the ring polymer melts would provide not only a new perspective to understand unsolved problems in biological systems but possibilities to utilize new materials with novel viscoelastic properties.

Bibliography

[1] Chanda, M.; Roy, S. K. *Industrial polymers, Specialty polymers and Their applications*; CRC Press, 2008.

[2] Berlin, A. A.; Kablov, V. F.; Pimerzin, A. A.; Zlotsky, S. S. *Key elements in polymers for engineers and chmists: from data to applications*; Apple Academic Press, 2014.

[3] Uchegbu, I. F.; Schatzlein, A. G. *Polymers in Drug Delivery*; CRC Press, 2006.

[4] Doi, M.; Edwards, S. F. *The theory of polymer dynamics*; Oxford: NY, United States, 1986.

[5] Grosberg, A. Y.; Khokhlov, A. R. *Statistical Physcis of Macromolecules*; AIP Press: NY, United States, 1994.

[6] Rubinstein, M.; Colby, R. H. *Polymer physics*; Oxford: NY, United States, 2003.

[7] Dulbecco, R.; Vogt, M. Evidence for a ring structure of polymer virus DNA. *Proc. Natl. Acad. Sci. USA* **1963**, *50*, 236–243.

[8] Vettorel, T.; Kremer, K. Territorial polymers. *Phys. Today* **2009**, *62*, 72.

[9] Brás, A. R.; Gooßen, S.; Krutyeva, M.; Radulescu, A.; Farago, B.; Allgaier, J.; Pyckhout-Hintzen, W.; Wischnewski, A.; Richter, D. Compact structure and non-Gaussian dynamics of ring polymer melts. *Soft Matter* **2014**, *10*, 3649–3655.

[10] Kremer, K.; Grest, G. S. Dynamics of entangled linear polymer melts: A molecular dynamics simulation. *J. Chem. Phys.* **1990**, *92*, 5057–5086.

[11] Mueller, M.; Wittmer, J. P.; Cates, M. E. Topological effects in ring polymers: A computational study. *Phys. Rev. E* **1996**, *53*, 5063–5074.

[12] Brown, S.; Szamel, G. Computer simulation study of the structure and dynamics of ring polymers. *J. Chem. Phys.* **1998**, *109*, 6184–6191.

[13] Brown, S.; Lenczycki, T.; Szamel, G. Influence of topological constraints on the statics and dynamics of ring polymers. *Phys. Rev. E* **2001**, *63*, 052801.

[14] Hur, K.; Winkler, R. G.; Yoon, D. Y. Comparison of ring and linear polyethylene from molecular dynamics simulations. *Macromolecules* **2006**, *39*, 3975–3977.

[15] Lee, E.; Kim, S.; Jung, Y. Solwing down of ring polymer dynamics caused by inter-ring threading. *Macromol. Rapid Commun.* **2015**, *36*, 1115–1121.

[16] Lee, E.; Jung, Y. *Soft Matter*, 2015, DOI: 10.1039/C5SM01097G.

[17] Mueller, M.; Wittmer, J. P.; Cates, M. E. Topological effects in ring polymers. 2. Influence of persistence length. *Phys. Rev. E* **2000**, *61*, 4078–4089.

[18] Halverson, J. D.; Lee, W. B.; Grest, G. S.; Grosberg, A. Y.; Kremer, K. Molecular dynamics simulation study of nonconcatenated ring polymers in a melt. 1. Statics. *J. Chem. Phys.* **2011**, *134*, 204904.

[19] Halverson, J.; Grest, G. S.; Grosberg, A.; Kremer, K. Rheology of ring polymer melts: From linear contaminant to ring-linear blends. *Phys.Rev.Lett.* **2012**, *108*, 038301.

[20] Rosa, A.; Everaers, R. Ring polymers in the melt state: The physics of crumpling. *Phys. Rev. Lett.* **2014**, *112*, 118302.

[21] Michieletto, D.; Marenduzzo, D.; Orlandini, E.; Alexander, G. P.; Turner, M. S. Dynamics of self-threading ring polymers in a gel . *Soft Matter* **2014**, *10*, 5936–5944.

[22] Cates, M. E.; Deutsch, J. M. Conjectures on the statics of ring polymers. *J. Phys. France* **1986**, *47*, 2121–2128.

[23] Sakaue, T. Ring polymers in melts and solutions: scaling and crossover. *Phys. Rev. Lett.* **2011**, *106*, 167802.

[24] Sakaue, T. Statistics and geometrical picture of ring polymer melts and solutions. *Phys. Rev. E* **2012**, *85*, 021806.

[25] Van Der Spoel, D.; Lindahl, E.; Hess, B.; Groenhof, G.; Mark, A. E.;

Berendsen, H. J. C. GROMACS: Fast, flexible, and free. *J. Comput. Chem.* **2005**, *26*, 1701–1718.

[26] Lieberman-Aiden, E. et al. Comprehensive mapping of long-range interactions reveals folding principles of the human genome. *Science* **2009**, *326*, 289–293.

[27] Sexton, T.; Yaffe, E.; Kenigsberg, E.; Bantignies, F.; Leblanc, B.; Hoichman, M.; Parrinello, H.; Tanay, A.; Cavalli, G. Three-dimensional folding and functional organization principles of the Drosophila genome. *Cell* **2012**, *148*, 458–472.

[28] Zhang, Y.; McCord, R. P.; Ho, Y.; Lajoie, B. R.; Hildebrand, D. G.; Simon, A. C.; Becker, M. S.; Alt, F. W.; Dekker, J. Spatial organization of the mouse genome and its role in recurrent chromosomal translocations. *Cell* **2012**, *148*, 908–921.

[29] Cremer, T.; Cremer, C. Chromosome territories, nuclear architecture and gene regulation in mammalian cells. *Nat. Rev. Genet.* **2001**, *2*, 292–301.

[30] Bolzer, A.; Kreth, G.; Solovei, I.; Koehler, D.; Saracoglu, K.; Fauth, C.; Mueller, S.; Eils, R.; Cremer, C.; Speicher, M. R.; Cremer, T. Three-dimensional maps of all chromosomes in human male fibroblast nuclei and prometaphase rossettes. *PLoS Biol.* **2005**, *3*, e157.

[31] Cremer, T.; Cremer, M.; Dietzel, S.; Mueller, S.; Solovei, I.; Fakan, S. Chromosome territories - a functional nuclear landscape. *Curr. Opin. Cell Biol.* **2006**, *18*, 307–316.

[32] van den Engh, G.; Sachs, R.; Trask, B. J. Estimating genomic distance from DNA sequence location in cell nuclei by a random walk model. *Science* **1992**, *257*, 1410–1412.

[33] Yokota, H.; van den Engh, G.; Hearst, J.; Sachs, R.; Trask, B. Evidence for the organization of chromatin in megabase pair-sized loops arranged along a random walk path in the human G0/G1 interphase nucleus. *J. Cell Biol.* **1995**, *130*, 1239–1249.

[34] Mateos-Langerak, J.; Bohn, M.; de Leeuw, W.; Giromus, O.; Manders, E. M. M.; Verschure, P. J.; Indemans, M. H. G.; Gieman, H. J.; Heermann, D. W.; van Driel, R.; Goetze, S. Spatially confined folding of chromatin in the interphase nucleus. *Proc. Natl. Acad. Sci.* **2009**, *106*, 3812–3817.

[35] Grosberg, A. Y.; Nechaev, S. K.; Shakhonovich, E. I. The role of topological constraints in the kinetics of collapse of macromolecules. *J. Phys. France* **1988**, *49*, 2095–2100.

[36] Grosberg, A. Y. Annealed lattice animal model and Flory theory for the melt of non-concatenated rings: towards the physics of crumpling. *Soft Matter* **2014**, *10*, 560–565.

[37] Schram, R. D.; Barkema, G. T.; Schiessel, H. On the stability of fractal globules. *J. Chem. Phys.* **2013**, *138*, 224901.

[38] Rosa, A.; Everaers, R. From a melt of rings to chromosome territories: the

role of topological constrints in genome folding. *PLoS Comput. Biol* **2008**, *4*, e1000153.

[39] Halverson, J. D.; Smrek, J.; Kremer, K.; Grosberg, A. Y. From a melt of rings to chromosome territories: the role of topological constrints in genome folding. *Rep. Prog. Phys.* **2014**, *77*, 022601.

[40] Olovnikov, A. M. A theory of marginotomy: The incomplete copying of template margin in enzymic synthesis of polynucleotides and biological significance of the phenomenon. *J. Theor. Biol* **1973**, *41*, 181–190.

[41] Greider, C. W.; Balckburn, E. H. A telomeric sequence in the RNA of Tetrahymema telomerase required for telomere repeat synthesis. *Nature* **1989**, *337*, 331–337.

[42] Wilson, O. C.; Olorunyolemi, T.; Jaworski, A.; Borum, L.; Young, D.; Siriwat, A.; Dickens, E.; Oriakhi, C.; Lerner, M. Surface and interfacial properties of polymer-intercalated layered double hydroxide nanocomposites. *Appl. Clay Sci.* **1999**, *15*, 265–279.

[43] Tsukruk, V. V.; Sidorenko, A.; Gorbunov, V. V.; Chizhik, S. A. Surface nanomechanical properties of polymer nanocomposite layers. *Langmuir* **2001**, *17*, 6715–6719.

[44] Smith, G. D.; Bedrov, D.; Borodin, O. Structural relaxation and dynamic heterogeneity in a polymer melt at attractive surfaces. *Phys. Rev. Lett.* **2003**, *90*, 226103.

[45] Daoulas, K. C.; Harmandaris, V. A.; Mavrantzas, V. G. Detailed atomistic simulation of a polymer melt/solid interface: structure, density and conformation of a thin film of polyethylene melt adsorbed on graphite. *Macromolecules* **2005**, *38*, 5780–5795.

[46] Virgiliis, A.; Milchev, A.; Rostiashvili, V. G.; Vilgis, T. A. Structure and dynamics of a polymer melt at an attractive surface. *Eur. Phys. J. E* **2012**, *35*, 97–107.

[47] Pandey, Y. N.; Doxastakis, M. Detailed atomistic Monte Calro simulations of a polymer melt on a solid surface and around a nanoparticles. *J. Chem. Phys.* **2012**, *136*, 094901.

[48] Roe, R. Multilayer theory of adsorption from a polymer solution. *J. Chem. Phys.* **1974**, *60*, 4192–4207.

[49] Scheutjens, J. M. H. M.; Fleer, G. J. Statistical theory of the adsorption of interacting chain molecules. 1. Partition function, segment density distribution, and adsorption isotherms. *J. Phys. Chem.* **1979**, *83*, 1619–1635.

[50] Scheutjens, J. M. H. M.; Fleer, G. J. Statistical theory of the adsorption of interacting chain molecules. 2. Train, loop and tail size distribution. *J. Phys. Chem.* **1980**, *84*, 178–190.

[51] Eisenriegler, E.; Kremer, K.; Binder, K. Adsorption of polymer chains at surfaces: Scaling and Monte Calro analyses. *J. Chem. Phys.* **1982**, *77*, 6296–6320.

[52] Carmesin, I.; Kremer, K. Static and dynamic properties of two-dimensional polymr melts. *J. Phys. France* **1990**, *15*, 919–932.

[53] Meyer, H.; Kreer, T.; Cavallo, A.; Wittmer, J. P.; Baschnagel, J. On the dynamics and disentanglement in thin and two-dimensional polymer films. *Eur. Phys. J.* **2007**, *141*, 167–172.

[54] Wittmer, J. P.; Meyer, H.; Johner, A.; Kreer, T.; Baschnagel, J. Algebraic displacement correlation in two-dimensional polymer melts. *Phys. Rev. E* **2010**, *105*, 037802.

[55] Meyer, H.; Wittmer, J. P.; Kreer, T.; Baschnagel, J. Static properties of polymer melts in two dimensions. *J. Chem. Phys.* **2010**, *132*, 184904.

[56] Halverson, J. D.; Lee, W. B.; Grest, G. S.; Grosberg, A. Y.; Kremer, K. Molecular dynamics simulation study of nonconcatenated ring polymers in a melt. 2. Dynamics. *J. Chem. Phys.* **2011**, *134*, 204905.

[57] van Lent, B.; Scheutjens, J.; Cosgrove, T. Self-consistent field theory for the adsorption of ring polymers from solution. *Macromolecules* **1987**, *20*, 366–370.

[58] Persson, F.; Utko, P.; Reisner, W.; Larsen, N. B.; Kristensen, A. Confinement spectroscopy: Probing single DNA molecules with tapered nanochannels. *Nano Lett.* **2009**, *9*, 1382–1385.

[59] Witz, G.; Rechendorff, K.; Adamcik, J.; Dietler, G. Conformation of ring polymers in 2D constrained enviornments. *Phys. Rev. Lett* **2011**, *106*, 248301.

[60] Reisner, W.; Morton, K. J.; Riehn, R.; Wang, Y. M.; Yu, Z.; Rosen, M.; Sturm, J. C.; Chou, S. Y.; Frey, E.; Austin, R. H. Static and dynamic of single DNA molecules confined in Nanochannels. *Phys. Rev. Lett.* **2005**, *94*, 196101.

[61] Benkova, Z.; Cifra, P. Simulation of semiflexible cyclic and linear chains moderately and strongly confined in nanochannels. *Macromolecules* **2012**, *45*, 2597–2608.

[62] Sheng, J.; Luo, K. Chain conformation of ring polymers under a cylindrical nanochannel confinement. *Phys. Rev. E* **2012**, *86*, 031803.

[63] Sakaue, T.; Witz, G.; Dietler, G.; Wada, H. Universal bond correlation function for two-dimensional polymer rings. *Europhys. Lett.* **2010**, *91*, 68002.

[64] Plimpton, S. Fast parallel algorithms for short-range molecular dynamics. *J. Comput. Phys.* **1995**, *117*, 1–19.

[65] Everasers, R.; Sukumaran, S. K.; Grest, G. S.; Svaneborg, C.; Sivasubramanian, A.; Kremer, K. Rheology and microscopic topology of entangled polymeric liquids. *Science* **2004**, *303*, 823–826.

[66] Hur, K.; Jeong, C.; Winkler, R. G.; Lacevic, N.; Gee, R. H.; Yoon, D. Y. Chain dynamics of ring and linear polyethylene melts from molecular dynamics simulations. *Macromolecules* **2011**, *44*, 2311–2315.

[67] Suzuki, J.; Takano, A.; Deguchi, T.; Matsushita, Y. Dimension of ring

polymers in bulk studied by Monte-Carlo simulation and self-consistent theory. *J. Chem. Phys.* **2009**, *131*, 144902.

[68] Vettorel, T.; Grosberg, A. Y.; Kremer, K. Statistics of polymer rings in the melt: a numerical simulation study. *Phys. Biol.* **2009**, *6*, 025013.

[69] DeYoung, A. D.; Park, S.-W.; Dhumal, N. R.; Shim, Y.; Jung, Y.; Kim, H. J. Graphene Oxide Supercapacitors: A Computer Simulation Study. *J. Phys. Chem. C* **2014**, *118*, 18472–18480.

[70] Silberberg, A. Distribution of conformations and chain ends near the surface of a melt of linear flexible macromolecules. *J. Colloid Interface Sci.* **1982**, *90*, 86–91.

[71] C.A.J.Goeve,; DiMarzio, E.; P.Peyser, Adsorption of polymer molecules at low surface coverage. *J. Chem. Phys.* **1965**, *42*, 2558.

[72] Sarabadani, J.; Milchev, A.; Vilgis, T. A. Structure and dynamics of polymer melts confined between two solid surfaces: A molecular dynamics study. *J. Chem. Phys.* **2014**, *141*, 044907.

[73] Bettorel, T.; Reigh, S. Y.; Yoon, D. Y.; Kremer, K. Monte-Carlo Method for Simulations of Ring Polymers in the Melt. *Macromol. Rapid Commun.* **2009**, *30*, 345.

[74] Kawaguchi, D.; Ohta, Y.; Takano, A.; Matsushita, Y. Temperature and Molecular Weight Dependence of Mutual Diffusion Coefficient of Cyclic Polystyrene/Cyclic Deuterated Polystyrene Bilayer Films. *Macromolecules* **2012**, *45*, 6748–6752.

[75] Kawaguchi, D. Direct observation and mutual diffusion of cyclic polymers. *Polym. J.* **2013**, *45*, 783–789.

[76] Rubinstein, M. Dynamics of Ring Polymers in the Presence of Fixed Obstacles. *Phys. Rev. Lett.* **1986**, *57*, 3023–3026.

[77] Thomas Vettorel, K. K. Development of entanglements in disentangled polymer melt. *Macromol. Theory Simul.* **2010**, *19*, 44–56.

[78] Michieletto, D.; Marenduzzo, D.; Orlandini, E.; Alexander, G. P.; Turner, M. S. Threading Dynamics of Ring Polymers in a Gel. *ACS Macro. Lett.* **2014**, *3*, 255–259.

[79] Jung, Y.; Garrahan, J. P.; Chandler, D. Dynamical exchanges in facilitated models of supercooled liquids. *J. Chem. Phys.* **2005**, *123*, 084509.

[80] Berthier, L.; Garrahan, J. Real space origin of temperature crossovers in supercooled liquids. *Phys. Rev. E* **2003**, *68*, 041201.

[81] Jeong, D.; Choi, M. Y.; Kim, H. J.; Jung, Y. Fragility, Stokes–Einstein violation, and correlated local excitations in a coarse-grained model of an ionic liquid. *Phys. Chem. Chem. Phys.* **2010**, *12*, 2001–2010.

[82] Hedges, L. O.; Maibaum, L.; Chandler, D.; Garahhan, J. P. Decoupling of exchange and persistence times in atomistic models of glass formers. *J. Chem. Phys.* **2007**, *127*, 211101.

[83] Tsolou, G.; Stratikis, N.; Baig, C.; Stephanou, P. S.; Mavrantzas, V. G. Melt structure and dynamics of unentangled polyethylene rings: Rouse

theory, atomistic molecular dynamics simulation, and comparison with the linear analogues. *Macromolecules* **2010**, *43*, 10692–10713.

국문 초록

원형 고분자는 새로운 위상 유형을 갖는 고분자의 한 종류이다. 원형 고분자는 선형 고분자, 분지 고분자와는 다르게 양쪽 끝이 서로 연결되어 있다. 따라서 서로 다른 두 분자들 사이에 얽히지 않고 하나의 분자에서 묶이지 않는 본질적인 위상 제한을 갖게 된다. 이러한 위상적 제한 때문에 원형 고분자의 구조는 높은 프랙탈 차원을 갖는 것으로 알려져 있다. 이 구조는 간기 세포의 염색체 구조와 매우 닮아있는데, 염색체는 양쪽 끝이 열려 있는 선형 고분자의 한 종류라는 점에서 매우 흥미롭다. 따라서, 원형 고분자의 물리적 현상 연구가 핵 내의 염색체 구조를 이해하는데 큰 도움이 될 수 있다.

최근 연구에 따르면 원형 고분자의 작은 플로리 지수는 위상적 제한 때문인 것으로 알려졌다. 특히 이러한 위상적 제한을 효과적 배제 부피로 표현하여 자유 에너지 최소화 과정을 거치면 중합도에 따라 원형 고분자의 플로리 지수가 달라짐을 확인할 수 있다. 특히 아주 긴 원형 고분자의 경우에는 이 지수가 1/3의 값을 가지며, 이는 분리되며 프랙탈 구상체의 구조를 의미한다. 이러한 이론적 결과를 분자동역학 시뮬레이션을 통해 확인할 수 있다.

또한 본 논문에서는 필름 내에 속박되어 있는 원형 고분자가 선형 고분자와 비교해 어떠한 구조를 갖는지에 대해 연구한다. 표면 근처에서 나타나는 정렬 구조의 경우 원형 고분자와 선형고분자에 크게 차이가 없는데 이는 원형 고분자를 이루고 있는 이상 블랍의 크기가 표면과 단위체 사이의 상호작용 거리보다 크기 때문이다. 하지만 조금 더 긴 거리에서는 원형 고분자와 선형 고분자 구조 사이에 큰 차이점이 나타나게 된다. 고분자의 크기 흡착량, 결합 수 등의 비교를 통해 원

형 고분자는 위상적 제외 부피 상호작용에 의해 속박되어있지 않은 경우보다 더 분리된 구상체의 구조를 갖는 것을 확인할 수 있다.

원형 고분자의 구조 뿐 아니라 그 동역학에서도 선형 고분자와 차이점이 나타난다. 원형 고분자는 선형 고분자와는 다르게 구조의 재배열 시간에 비해 확산 시간이 매우 느린 것으로 알려져 있다. 또한 선형 고분자에서 나타나는 얽힘 구조에 대한 증거 또한 밝혀진 바가 없다. 원형 고분자는 고분자의 끝이 서로 연결되어 있기 때문에 엮임 구조를 정의하기조차 매우 힘들다. 따라서 본 논문에서는 분자 동역학 시뮬레이션과 분자 접촉의 지속 및 교환시간 분포 분석을 통해 엮임 현상 때문에 원형 고분자의 확산이 느려짐을 보인다.

이와 같은 원형 고분자의 구조 및 동역학에 대한 연구는 생물학적 계에 대한 이해를 도울 뿐 아니라 새로운 점탄성을 지니는 물질의 합성 연구에도 도움을 줄 수 있다.

주요어: 고분자 물리, 원형 고분자, 분리된 구조, 프랙탈 구상체, 실버버그 가설, 위상적 배제 부피 상호작용, 엮임 동역학, 얽힘 효과, 염색체 쌓임, 지속/교환 시간
학번: 2008-22732